Retrieval Algorithm for Aerosol Effective Height from the Geostationary Environment Monitoring Spectrometer (GEMS)

Sang Seo Park[1,*], Jhoon Kim[2], Yeseul Cho[2], Hanlim Lee[3], Junsung Park[3], Dong-Won Lee[4], Won-Jin Lee[4], Deok-Rae Kim[4]

[1] *Department of Urban and Environmental Engineering, Ulsan National Institute of Science and Technology, Ulsan, Korea*

[2] *Department of Atmospheric Sciences, Yonsei University, Seoul, Korea*

[3] *Division of Earth and Environmental System Sciences, Pukyong National University, Busan, South Korea*

[4] *Envionment Satellite Center, National Institute of Environmental Research, Incheon, Korea*

[*] Corresponding author. Sang Seo Park (sangseopark@unist.ac.kr)

Submitted to Atmospheric Measurement Techniques

2023. 06.

Abstract

An algorithm for aerosol effective height (AEH) was developed for operational use with observations from the Geostationary Environment Monitoring Spectrometer (GEMS). The retrieval technique uses the slant column density of the oxygen dimer (O_2-O_2) at 477 nm, which is converted into AEH after retrieval of aerosol and surface optical properties from GEMS operational algorithms. The AEH retrieval results show significant AEH values and continuously monitor aerosol vertical height information in severe dust plumes over East Asia, and the collection of plume height information for anthropogenic aerosol pollutants over India. Compared to the AEH retrieved from Cloud-Aerosol Lidar with Orthogonal Polarization (CALIOP), the retrieval results show bias of -0.03 km with a standard deviation of 1.4 km for the AEH difference over the GEMS observation domain from January to June, 2021. The AEH difference depends on aerosol optical properties and surface albedo. Compared to the aerosol layer height obtained from the tropospheric monitoring instrument (TROPOMI), differences of 1.50 ± 1.08 km, 1.59 ± 1.22 km, and 1.71 ± 1.24 km were obtained for pixels with single scattering albedo (SSA) < 0.90, 0.90 < SSA < 0.95, and SSA > 0.95, respectively, with significant dependence on aerosol type.

Keywords: aerosol effective height, aerosol optical depth, environmental satellite, GEMS

1. Introduction

Since the launch of the Total Ozone Mapping Spectrometer (TOMS) on Nimbus-7, ultraviolet (UV)-visible satellite measurements have been used for environmental monitoring of the distribution and reaction processes of pollutants (e.g., anthropogenic aerosols, tropospheric ozone, NO_2, and SO_2). Measurements from environmental satellites have been used to estimate gaseous species in the atmosphere, resulting in vertical column integrated amounts. However, these column-integrated amounts and associated surface concentrations have uncertainty due to simultaneous changes in optical path length associated with the vertical distribution of target species and amounts of scattering materials (clouds and aerosols) present. In addition, aerosol vertical information is also important information for the application. For example, aerosol height information in the free troposphere is particularly important for aviation safety by affecting the visibility. Also, scientific applications including radiative forcing studies, long-range transport modelling and studies of cloud formation processes have been used aerosol vertical information as an input parameter.

Environmental satellite sensors, in particular those that measure UV-visible wavelength range, have been used the UV aerosol index (UVAI) for aerosol detection (e.g., Buchard *et al.*, 2015; Herman *et al.*, 1997; Torres *et al.*, 1998, 2002; Prospero *et al.*, 2000; de Graaf *et al.*, 2005). Furthermore, scattering radiative index values were investigated for the possibility of the cloud signal detection (Penning de Vries *et al.*, 2009, 2015; Kooreman *et al.*, 2020; Kim *et al.*, 2018). However, these indices only have qualitative characteristics and limitations to identify aerosol amounts.

For the quantitative estimation, measurements of aerosol optical depth (AOD) and radiative cloud fraction have also been retrieved from pixel-based radiance data in UV-visible wavelength range. Recently, various aerosol retrieval algorithms have been developed in order to be applied in passive satellite sensors. These algorithms focus on improved trace gas retrieval as well as direct monitoring of aerosol properties, such as AOD and single scattering albedo (SSA) (e.g., Ahn *et al.*, 2014; Kim *et al.*, 2020; Torres et al., 2020).

Although the algorithms developed for environmental satellite sensors indicate the presence and amount of scattering materials, the accuracy of these retrieval algorithms for trace gases is affected by the relative vertical distributions between trace gases and scattering materials (e.g., Lorente *et al.*, 2017; Hong *et al.*, 2017). For this reason, estimating cloud vertical parameters is important. For cloud vertical information, cloud height information has been estimated simultaneously with cloud optical depth and radiative cloud fraction data using the rotational Raman scattering (Joiner and Vasilkov, 2006; Vasilkov *et al.*, 2008; Joiner and Bhartia, 1995) and absorption intensity of the oxygen dimer (O_2-O_2) (Accarreta *et al.*, 2004; Vasilkov *et al.*, 2018; Choi *et al.*, 2021) combined with normalized radiance.

Similarly, the aerosol vertical distribution can be estimated using the oxygen absorption bands, such as the O_2-O_2 (Park *et al.*, 2016; Chimot *et al.*, 2017; Choi *et al.*, 2019, 2020), O_2-A (Dubisson *et al.*, 2009; Geddes and Boesch, 2015; Sanders *et al.*, 2015; Zeng *et al.*, 2020), and O_2-B (Ding *et al.*, 2016) bands, as well as combinations of these bands (Sanghavi *et al.*, 2012; Chen et al., 2021). In addition, an algorithm for aerosol vertical information has been developed based on hyperspectral UV-visible radiance from satellite observation. Nanda *et al.* (2018) demonstrated the possibility of aerosol height retrieval from the O_2-A band developed an algorithm using Tropospheric Monitoring Instrument (TROPOMI) (Sanders and de Haan, 2016; Nanda *et al.*, 2020) and implemented the algorithm operationally.

However, the vertical distribution of aerosol is difficult to assess because of its large spatio-temporal variability. Although the Cloud-Aerosol Lidar with Orthogonal Polarization (CALIOP) provided the aerosol vertical distribution with high vertical resolution (Omar et al., 2009), other passive satellite sensors are only able to estimate the representative parameter of aerosol height. Veihelmann et al. (2007) showed that the number of degrees of freedom of signal for aerosol is 2~4 for most of satellite observation conditions by the ozone monitoring instrument (OMI). In addition, the number of degrees of freedom is not exceeded to 3 from the shortwave satellite measurements (e.g., Rao et al., 2019; Choi et al., 2021). It means that the amount of information for aerosol vertical distribution has a limitation for satellite sensor. Because of limitation for describing the aerosol vertical information, aerosol layer height (ALH) (Nanda et al., 2018) or aerosol effective height (AEH) (Park et al., 2016) were defined to retrieve the aerosol vertical information from the passive satellite sensors.

The Geostationary Environment Monitoring Spectrometer (GEMS), which was launched by South Korea in February 2020, retrieves data related to major trace gases and aerosol properties (Kim *et al.*, 2020). The main purpose of GEMS is to monitor air quality, and aerosol properties are targets of such monitoring over East Asia. For this reason, the GEMS aerosol algorithm was developed as multiple operational products. Aerosol properties are obtained for the purposes of monitoring surface air quality and aerosol effects for the air mass factor (AMF) calculation. In addition to the aerosol optical property algorithm, the GEMS aerosol product is applied to the aerosol vertical information, AEH. For the possibility for development of an AEH retrieval algorithm, Park *et al.* (2016) conducted theoretical sensitivity testing of AEH retrieval using solely the O_2-O_2 absorption band along with aerosol and surface properties. Overall, the sensitivity of AEH retrieval was strongly affected by SSA, AOD, and aerosol types including optical and size properties, and the error budget for AEH retrieval using the O_2-O_2 band was 739 ~ 1276 m. In addition, case studies of AEH during dust transport over East Asia were conducted using radiance data from the Ozone Monitoring Instrument (OMI) and aerosol optical properties from the Moderate Resolution Imaging Spectroradiometer (MODIS).

Based on theoretical considerations and case results of previous studies, we introduce an operational retrieval algorithm for AEH. Section 2 introduces the details of satellite sensors for the comparison and colocation method in this study. Section 3 describes the details of the AEH retrieval algorithm for GEMS and provides a list of the detailed input parameters. Section 4 reports retrieval results based on case studies of aerosol transport, and section 5 contains long-term validation results based on Cloud-Aerosol Lidar with Orthogonal Polarization (CALIOP) and TROPOMI data. Finally, we show conclusion and summary in section 6.

2. Data

2.1 GEMS

The GEMS is onboarding the Geostationary Korea multipurpose satellite 2B (GK2B) as orbiting at 128.2°E, and scans from 145°E to 75°E with north-south coverage of 5°S~45°N. The GK2B observation schedule shares the GEMS and the Geostationary Ocean Color Imager 2 (GOCI2), and the GEMS scan the 30 minutes duration from every hour from 45 minutes to 15 minutes during daytime. The standard spatial resolution of GEMS is 7 km × 8 km. The spectral resolution and sampling are respectively 0.6 nm with full-width and half-maximum (FWHM) and 0.2 nm with spectral range of 300~500 nm.

The GEMS Level 2 aerosol operational algorithm (L2AERAOD) retrieves the aerosol index (AI) values for UV and visible wavelengths, as well as AOD and SSA with considering the aerosol types (National Institute of Environmental Research, 2020a). The aerosol types are defined as absorbing, non-absorbing, and dust types by using the classification methods based on the UV and visible AIs (e.g., Go et al., 2020). Park *et al.* (2016) noted that the error budget of AEH is significantly affected by uncertainty in AOD and SSA and by the misclassification of aerosol types, which is directly related to the optical property and size information. Overall, the error for AEH is ranged from 739~1276 m under the AOD error of 0.2, particle size error of 20%, SSA error of 10%, and surface albedo error of 0.02 (Park et al., 2016). The main variables causing errors for AEH retrieval can be obtained from the L2AERAOD results. Therefore, the L2AERAOD results for AOD at 550 nm and SSA at 443 nm were adopted as input data for aerosol properties.

Although L2AERAOD retrieved their own surface reflectance for accurate separation of surface signals from total reflectance at the top of the atmosphere (TOA), the standard product for surface reflectance (L2SFC) (National Institute of Environmental Research, 2020b) was also independently retrieved from GEMS radiance/irradiance data with specific temporal periods. L2SFC is the reference product for spectral surface reflectance. The L2SFC retrieves the surface reflectivity in multiple spectral channels and provides the black surface reflectivity (BSR) and bi-directional reflectance distribution function (BRDF) based on the original pixel resolution. Recently, L2SFC accurately estimated surface reflectance in near real time in operation. For this reason, L2SFC was used as reference data for the surface products for all trace gas retrieval algorithms. Similarly, the AEH retrieval algorithm also uses L2SFC as a reference surface property in operation. Specifically, the BSR value at 477 nm is used as the surface reflectance input for AEH retrieval. However, this study used the minimum reflectance under the Lambertian assumption to retrieve AOD and AEH to coincide with the use of surface information on L2AERAOD and AEH retrieval.

2.2. TROPOMI

TROPOMI is a nadir-viewing spectrometer, the only payload of the Sentinel-5 Precursor (S5P), measuring radiance in the UV, visible, near-infrared, and the shortwave IR (Veefkind et al., 2012). The S5P crosses the equator at 13:30 local time in a polar orbit with ascending node providing near-global daily coverage. The aerosol layer height product from TROPOMI (AER_LH) retrieves vertically localized aerosol layers in free troposphere with cloud free condition by using the level 1b earth radiance measurements from 758 to 770 nm (de Graaf *et al.*, 2022). The definition of ALH from TROPOMI is the optical centroid layer height of the plume above sea level. Spectral fit estimation of reflectance around the O_2-A band is based on a neural network for the forward model calculation for simulated condition. After cloud masking to avoid the cloud affected pixels, an optimal estimation method was used to retrieve the aerosol layer height parameters for the inversion method from observation. During the radiance fitting, the ALH and AOD are fitted parameters, but other aerosol parameters, such as SSA, layer thickness, and scattering phase function, are assumed to be fixed values (Nanda et al., 2020). Furthermore, the ALH retrieval has limitation to the aerosol plume with higher than 12 km, because the ALH neural network method is currently adopted to the plume pressure range of 75~1000 hPa (Michailidis et al., 2023).

Main purpose of the AER_LH product is the retrieval of aerosol layers in the free troposphere (desert dust, biomass burning, and volcanic ash) (Michailidis et al., 2023). The target requirement on the accuracy and precision is 0.5 km or 50 hPa, and the threshold requirement is 1 km or 100 hPa under the elevated aerosol plumes with cloud-free conditions (de Graaf et al., 2022, Veefkind et al., 2012). From Michailidis et al. (2023), a mean bias of -0.51±0.77 and -2.27±1.17 km is estimated over ocean and land, respectively. In addition, the TROPOMI ALH product has strong dependence of the surface albedo, especial to the bright surfaces (Sanders et al., 2015). Furthermore, experimental retrieval range of ALH from TROPOMI is 0.27~6.5 km and 0.06~2.15 km over ocean and land, respectively. It has strong retrieval dependence of surface types (Michailidis et al., 2023). In this study, we use version 02.04.00 of the TROPOMI offline level 2 AER_LH product (European Space Agency, 2021) with the spatial resolution is 3.5 km × 5.5 km at nadir viewing geometry.

2.3. CALIOP

The CALIOP is a spaceborne lidar onboard the Cloud-Aerosol Lidar and Infrared Pathfinder Satellite Observations (CALIPSO) to measure the vertical information of aerosol and cloud with estimating the optical properties. The CALIOP has two different wavelength channels (532 and 1064 nm) by using the Nd:YAG laser to generate the signals (Winker et al., 2009). The orbit for CALIPSO is Sun synchronous orbit constellated to the A-train with period of 98.3 minutes by ascending node. It crosses the equator at 13:30 local time. For the vertical information, the resolution for vertical sampling is 30 m below 8 km altitude, and 60 m from 8 to 20 km altitude, respectively.

Although the CALIOP retrieves the data with extremely high horizontal and vertical resolutions, the spatial coverage is narrow because the footprint of the CALIOP is about 90m at the Earth surface. In this study, the data of Level 2 aerosol profile product (APro, version 3.41) was used. The AOD from CALIOP is vertically integrated aerosol extinction coefficient from surface to top of atmosphere, and representative layer height parameters (ALH and AEH) are directly estimated by using the vertical profile of aerosol extinction coefficient at 532 nm to minimize the spectral discrepancy of aerosol extinction.

2.4 Data Selection and Colocation

For spatial colocation, we selected pixels for which distance between GEMS and CALIOP (or TROPOMI) observations was less than 50 km. From Park et al. (2020), the spatial scales for AOD validation are 30~40 km. To secure the number of observation pixels, we mitigate the spatial scale condition for the colocation. In addition, only the closest 10% of pixels were used. Given the different orbital characteristics of CALIOP (or TROPOMI) and GEMS, temporal colocation was also considered. During the period of image scanning from east to west over Asia by GEMS, CALIOP and TROPOMI pass through the GEMS observation area from south to north every 98.3 minutes. On average, two low earth orbit (LEO) satellites pass three to four orbits through the GEMS scan area during a single day of daytime observation. To consider these different orbital characteristics, only observations taken within ±1 hour of the GEMS observation time was selected for temporal colocation. As GEMS observes hourly, collocated pixels between the two satellites shift from east to west over time.

To ensure the accuracy of ALH from TROPOMI, in addition, only pixels with quality assurance (QA) values of 1.0 were used. To minimize the cloud contamination, the TROPOMI ALH product uses the VIIRS cloud mask information and cloud parameters from the Fast Retrieval Scheme for Clouds from the Oxygen A-band (FRESCO). To consider the cloud contamination for the aerosol products, the VIIRS cirrus cloud reflectance (viirs_cirrus_reflectance < 0.4), VIIRS cloud mask (viirs_cloud_mask < 0.1), and cloud fraction from the FRESCO (cloud_fraction < 0.1) are considered in this study (Michailidis et al., 2023). However, de Graaf *et al.* (2022) showed that respective cloud masking method have difficulty detecting various clouds. For this reason, accuracy problem of ALH by the cloud contamination is remained. From the previous studies, the UVAI is used as the threshold to define the absorbing aerosol pixels (e.g., Chen et al., 2021; Griffin et al., 2020; Michailidis et al., 2023; Sanders et al., 2015). However, the GEMS aerosol product is retrieved not only the absorbing aerosols, but also the non-absorbing aerosols. For this reason, the UVAI is not used to the threshold of aerosol pixel identification.

3. AEH retrieval algorithm

AEH is a layer height parameter that considers the penetration of photons into the aerosol layer. In this study, the AEH product from GEMS is defined as the height with aerosol extinction integrated from the surface of (1-exp^{-1}) × AOD, and a detailed definition of AEH was introduced by Park *et al.* (2016). Numerous previous studies have used the aerosol top layer height (Kohkanovsky and Rozanov, 2010) or middle layer height (i.e. ALH or centroid height) (e.g., Sanders *et al.*, 2015; Nanda *et al.*, 2020) as the aerosol vertical layer parameter. AEH is similar to the aerosol top layer height but with a slight bias.

For AEH retrieval, the vertical distribution assumption is also important. The Gaussian Density Fitting (GDF) distribution, which is a modified Gaussian distribution structure, is assumed for AEH retrieval. The full-width at half-maximum (FWHM) of the aerosol layer is 1 km. Schematic description of AEH and other aerosol vertical parameters are shown in Figure 1. Based on the assumptions about the aerosol vertical distribution, the AEH value is greater than the peak height of the Gaussian distribution and lower than the aerosol top layer height. Otherwise, aerosol layer height (ALH) in this study is defined as the height integrated aerosol extinction from the surface reaching half of AOD (i.e., 0.5 × AOD). Therefore, the ALH is same to the peak height for the vertical profile condition as shown in Figure 1.

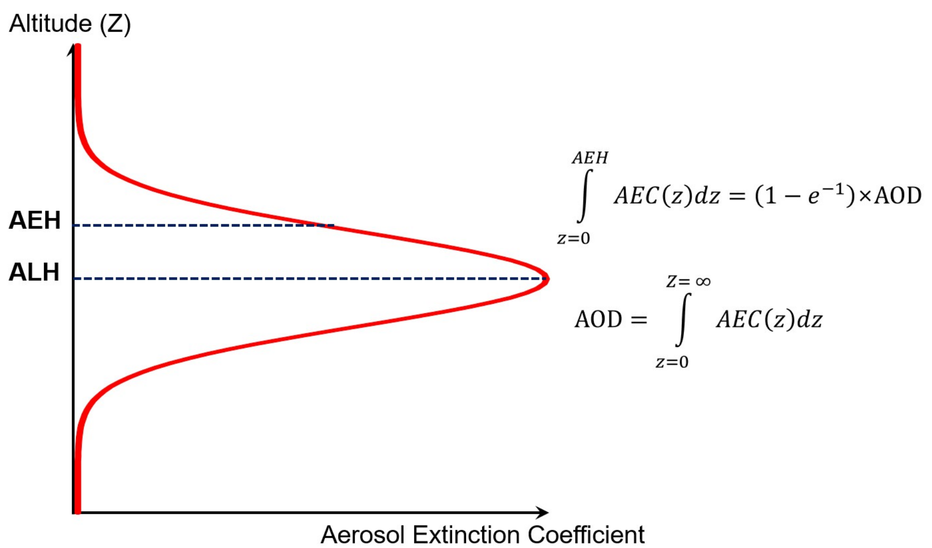

Figure 1. A schematic illustration of AEH and ALH definitions in an idealized Gaussian shape of aerosol vertical distribution.

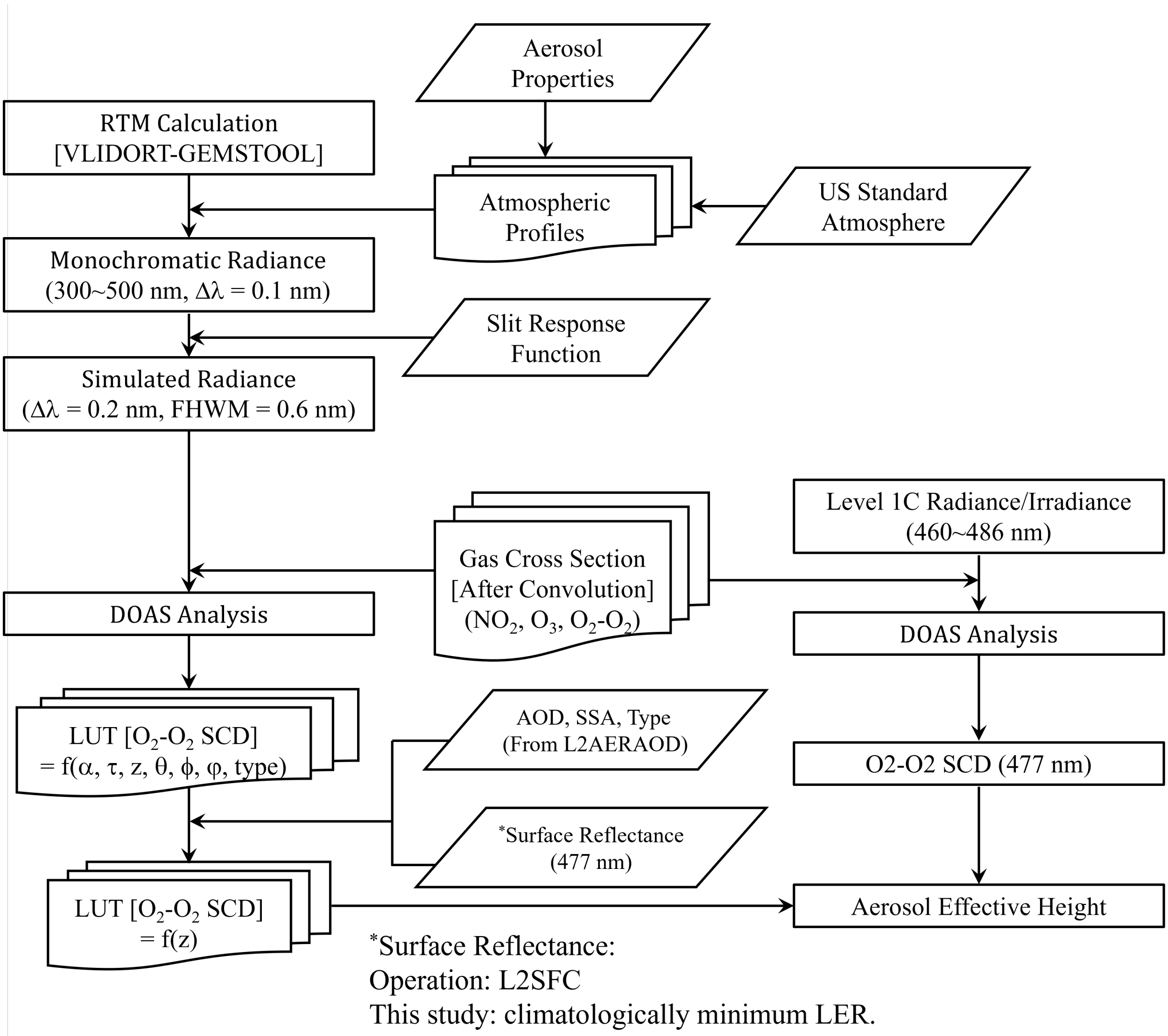

Figure 2. Flowchart of the AEH retrieval algorithm for GEMS satellite observation.

Figure 2 shows the overall flowchart of the AEH algorithm for GEMS satellite. The AEH algorithm for GEMS composed a look-up table (LUT) development between AEH and O_2-O_2 SCD by the radiance simulation and SCD estimation from the satellite radiance. The LUT is a function of observation geometries [solar zenith angle (SZA; θ), viewing zenith angle (VZA; Φ), relative azimuth angle (RAA; φ)], surface altitude (z), surface albedo (α), AOD (τ), and aerosol type. During the radiance simulation, the radiance is monochromatically simulated and simulated monochromatic radiance is convolved as considering the spectral response of GEMS instruments. For AEH estimation, the radiance information is finally converted to the AEH values by using the differential optical absorption spectroscopy (DOAS) method. DOAS method is identification technique for the spectral absorption signals from radiance information and detailed principle and information is explained by Platt (1994). DOAS method has been frequently used to estimate the amount of trace gases (i.e., SCD of trace gas) from ground (e.g., Cheng et al., 2023; Irie et al., 2008; Platt and Stutz, 2008; Wagner et al., 2011; Wang et al., 2017) and satellite (e.g., Kwon et al., 2019; Li et al., 2023; Wagner et al., 2007, 2010) measurements.

For AEH retrieval, the basic method is the identification of changes in optical path length caused by effective aerosol layer height variation. To measure the optical path length change, O_2-O_2 slant column density (SCD) retrieved by the DOAS method was used because the spectral coverage is limited to 300-500 nm (Park et al., 2016, Kim et al., 2020). In the GEMS product, the O_2-O_2 SCD at 477 nm absorption band is most useful absorption band because this absorption band is strongest absorption band within the GEMS spectral observation range. Detailed DOAS fitting parameter and setting information is provided in Table 1 for the estimation of O_2-O_2 SCD from both the simulation and observation data. For the O_2-O_2 SCD estimation at 477 nm, the fitting window is ranged from 460 to 486 nm to cover the full absorption structure of O_2-O_2. Within the fitting window, the absorptions of NO_2 and O_3 is significant. To describe these two absorbing species, temperature dependent cross section information are adopted. The temperature dependent cross section setting considers the stratosphere and troposphere, simultaneously.

Table 1. Details of fitting parameter for O_2-O_2 SCD estimation via the DOAS method.

Parameter	
Fitting window	460 – 486 nm
Absorption cross section	NO_2 at 220 and 294 K (Vandaele *et al.*, 1998) O_3 at 223, 243 and 293K (Bogumil *et al.*, 2001) O_2-O_2 at 293 K (Thalman and Volkamer, 2013) Ring

Table 2. Ratio between SCD error and the SCD of O_2-O_2 according to the polynomial order and offset settings used for DOAS fitting.

Polynomial	Offset = none	Offset = 0^{th}
2^{nd} order	6.06 ± 2.07	6.79 ± 2.31
3^{rd} order	6.32 ± 2.20	6.79 ± 2.32
4^{th} order	7.86 ± 2.78	7.34 ± 2.85

To minimize the noise effect and improve fitting quality, the optimal settings for fitting were also analyzed. Table 2 shows ratios of SCD error to the SCD for various polynomial and bias orders from observed radiance. The polynomial and offset are basic fitting parameters for the DOAS fitting. Two parameters describe the broadband spectral feature of radiance before identifying the gas absorption structure. The ratio between SCD error and the SCD of O_2-O_2 is important to determine the AEH retrieval quality. When the fitting error increase, the uncertainty of AEH is also enhanced during the retrieval. Although the fitting quality was good overall, the setting with 2^{nd} order of polynomial and none offset was used for the O_2-O_2 SCD estimation from the GEMS radiance due to the smallest fitting error.

In AEH estimation, other aerosol characteristics, including aerosol load and optical properties, affect retrieval accuracy. From Park et al. (2016), uncertainty of AEH retrieval result is largest by the SSA uncertainty. In addition, the AEH retrieval uncertainty by the aerosol optical properties and surface albedo has dependence of observation geometries. After the estimation of O_2-O_2 SCD, for this reason, conversion from O_2-O_2 SCD to AEH is an essential process. Table 3 shows the dimension of the LUT for the AEH retrieval algorithm. To calculate the LUT, a linearized pseudo-spherical vector discrete ordinate radiative transfer model (VLIDORT) version 2.6 was used (Spurr, 2013). During the radiative transfer model simulation, reference wavelength for the SSA and AOD is assumed to be 440 nm. The aerosol type is considered by the radiative absorptivity and size information, which is based on the method from Lee et al. (2010). Based on the Lee et al. (2010), the aerosol type is classified to absorbing, dust, and non-absorbing aerosol. Absorbing and non-absorbing aerosol types are assumed to the fine-mode dominant particles. For the spectral conversion of AOD, the angstrom exponent of 1.186, 0.222, and 1.179 are used for absorbing, dust, and non-absorbing aerosol, respectively. Otherwise, the SSA is assumed as the fixed value within the spectral range for O_2-O_2 estimation. Although the center of O_2-O_2 absorption is 477 nm, the spectral discrepancy between model assumed wavelength and center wavelength of O_2-O_2 absorption is assumed to be ignored in this study. After calculating spectral radiance with 0.1 nm sampling, we performed the slit response function of GEMS and sampling specification prior to the DOAS fitting. For O_2-O_2 absorption, the absorption cross section used for the radiative transfer model calculation is considered the temperature dependent absorption cross section (e.g., Park *et al.*, 2017).

Table 3. The dimension of the LUT for the GEMS AEH retrieval algorithm used to estimate AEH from O_2-O_2 SCD. (SZA: solar zenith angle, VZA: viewing zenith angle, RAA: relative azimuth angle, SUR: surface reflectance).

<table>
<tr><th>Variable [unit]</th><th>No. of entries</th><th colspan="2">Entries</th></tr>
<tr><td>Spectral range [nm]</td><td>-</td><td colspan="2">455~491 nm (0.1 nm interval)</td></tr>
<tr><td>SZA [º]</td><td>7</td><td colspan="2">0.01, 10, 20, 30, 40, 50, 60</td></tr>
<tr><td>VZA [o]</td><td>7</td><td colspan="2">0.01, 10, 20, 30, 40, 50, 60</td></tr>
<tr><td>RAA [o]</td><td>10</td><td colspan="2">0.01,20, 40, 60, 80, 100, 120, 140, 160, 180</td></tr>
<tr><td>SUR</td><td>3</td><td colspan="2">0.0, 0.05, 0.2</td></tr>
<tr><td>AOD at 440 nm</td><td>11</td><td colspan="2">0.04, 0.2, 0.4, 0.7, 1.0, 1.3, 1.6, 2.0, 2.5, 3.0, 5.0</td></tr>
<tr><td rowspan="3">Refractive Index (Imaginary) at 440 nm</td><td rowspan="3">3×3</td><td>Absorbing
(Real: 1.45)</td><td>0.000, 0.0074, 0.0314</td></tr>
<tr><td>Dust
(Real: 1.53)</td><td>0.0, 0.0030, 0.0080</td></tr>
<tr><td>Non-Absorbing
(Real: 1.41)</td><td>0.0, 0.0040, 0.0156</td></tr>
<tr><td>AEH [km]</td><td>13</td><td colspan="2">0.0 (Extrapolate), 0.2, 0.5, 1.0, 1.3,1.6, 2.0, 2.3, 2.7, 3.0, 3.5, 5.0, 10.0 (Extrapolate)</td></tr>
<tr><td>Terrain Height [km]</td><td>2</td><td colspan="2">0.0, 2.0</td></tr>
</table>

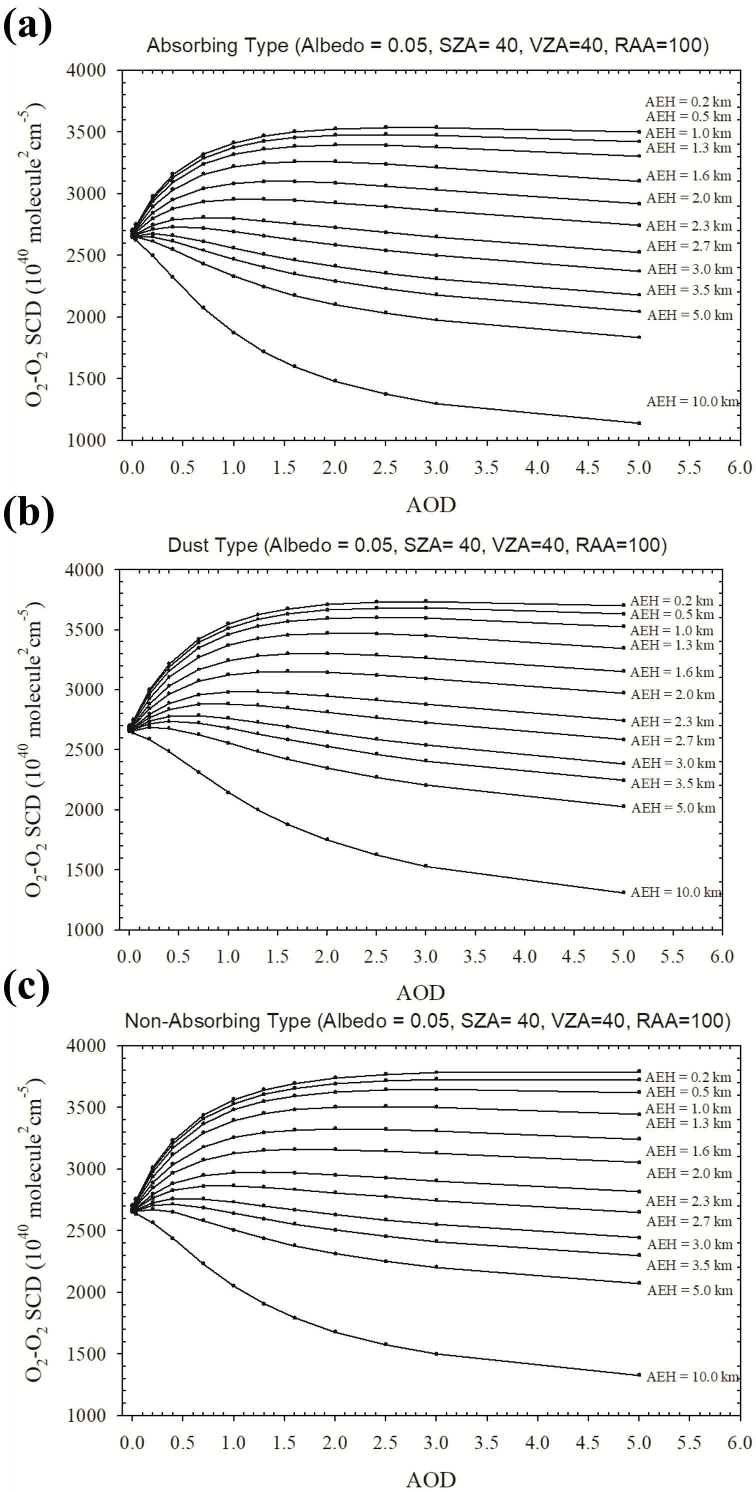

Figure 3. Example of LUT to retrieve the AEH according to (a) Absorbing, (b) Dust, and (c) Non-Absorbing aerosol types.

Figure 3 shows the example of LUT to retrieve the AEH from O_2-O_2 SCD according to the respective aerosol types and AOD. O_2-O_2 SCD decreases with increasing AEH for all aerosol types and AOD (Park *et al.*, 2016). Similar to the previous study, the O_2-O_2 SCD sensitivity is enhanced at high AOD and absorbing aerosol cases from GEMS LUT. In addition, the contrast of O_2-O_2 SCD is greater for absorbing aerosols than non-absorbing aerosols. During the radiance passing through the aerosol layer, the absorbing aerosol is more efficiently absorbed the radiance. For this reason, the effective optical path length is significantly shorter for absorbing aerosols. Overall, Park et al. (2016) reported the total error of AEH retrieval using O_2-O_2 band is 0.74~1.28 km with dependence of aerosol types. Based on the changes in sensitivity observed for optical path length, aerosol type (in particular in terms of SSA) and AOD, and surface reflectance are considered as input parameters for AEH retrieval. As shown in Section 2.1, the L2SFC product is used in operation, but this study used the climatological minimum Lambertian surface reflectance.

4. Case studies

Figure 4 shows retrieval results for AEH from GEMS on March 29 over East Asia. Because the operational schedule is hourly during the daytime, the GEMS retrieval results are shown at 1-hour intervals from 01:00 to 07:00 Universal Time Coordinated (UTC). AOD and SSA are also shown in Figures S1 and S2, respectively. From Park et al. (2016), pixels with low AOD values have large AEH uncertainty due to weak aerosol scattering information. For this reason, only AEH retrieval results with AOD greater than 0.3 are shown in this study. During this case study, a yellow dust plume was located along the coast of China and South Korea with AOD at 443 nm of 0.8~1.2.

Simultaneously, another plume was also present over the northeastern Korean Peninsula with AOD of 1.0~2.0 at 443 nm. SSA at 443 nm was 0.90~0.93 for the plume over South Korea and 0.87~0.90 for the plume over the northeastern Korean Peninsula. Retrieved AEH results from these different plumes show similar ranges. For both detected plumes, the AEH shows similar pattern ranging between 1.0 to 2.0 km in this case.

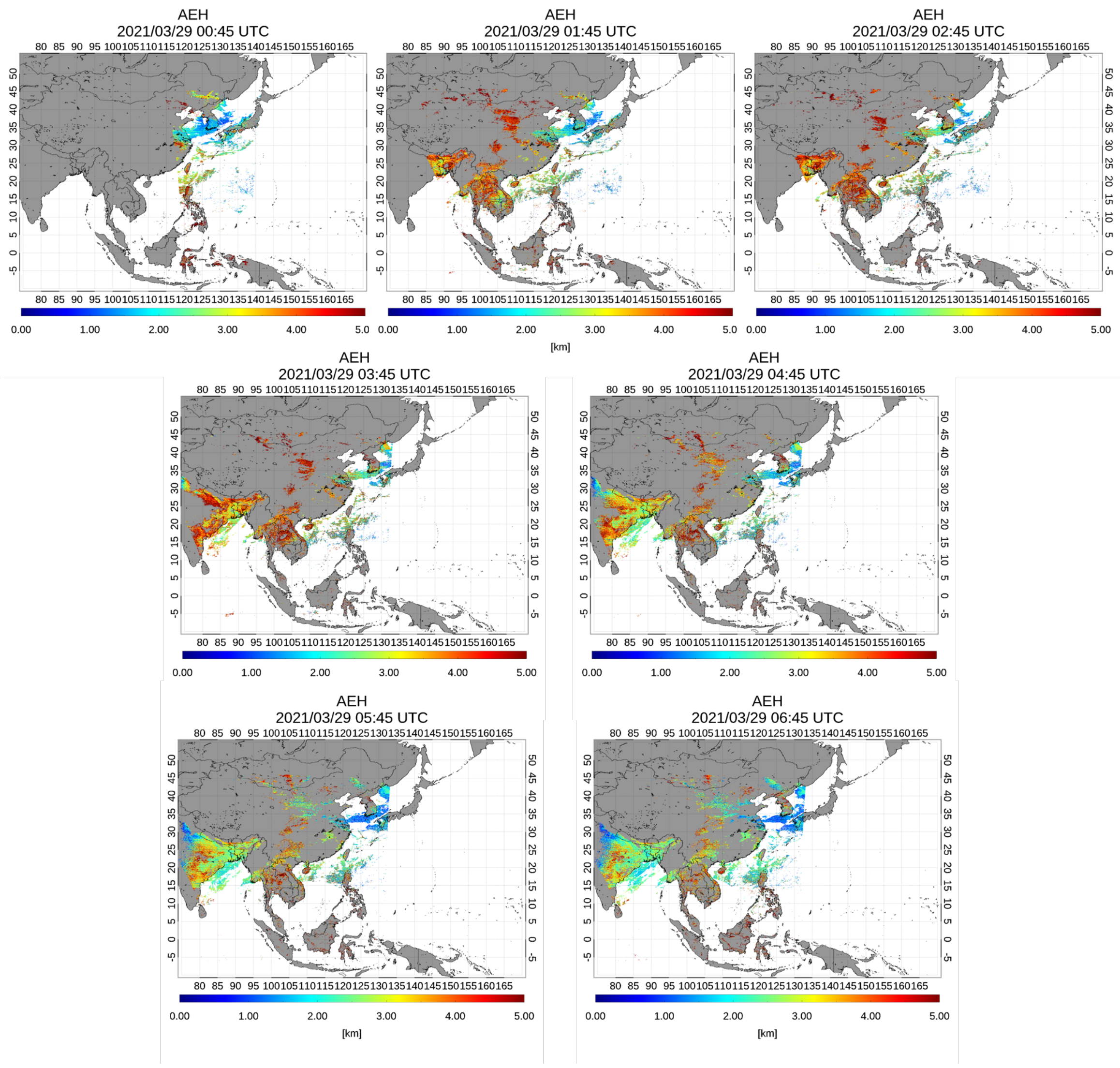

Figure 4. Case study results for AEH based on GEMS observations on March 29, 2021.

An additional severe aerosol plume was present over northeastern India, with AOD at 443 nm of 1.0~2.0 and SSA at 443 nm of 0.85~0.90. From Rana *et al.* (2019), metropolitan cities and industrial cluster in India are heavy emitters of black carbon, and high concentrations of black carbon are distributed over the Indo-Gangetic Plain (IGP). Therefore, the aerosol plume with high AOD and low SSA (high absorbing) was a result that actually exists, and it was not a result with high uncertainty due to edge of GEMS observation field. Except for the inland parts of India, AEH in high AOD pixels ranged from 1.5 to 3.5 km.

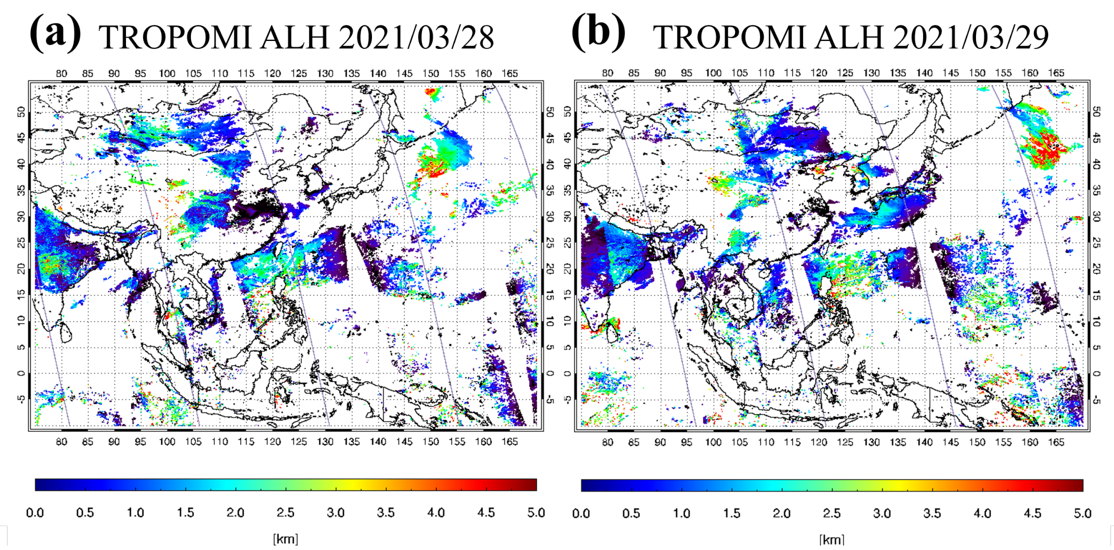

Figure 5. ALH retrieved from TROPOMI and orbit path of CALIOP on (a) March 28 and (b) March 29, 2021 (Unit: km).

For comparison of the retrieval, Figure 5 shows the ALH retrieved from TROPOMI on March 28 and 29, 2021 over East Asia. A dust plume was transported from China to South Korea during this period, then split into two distinct plumes over northeastern China and the coastal area of South Korea. The ALH retrieved from TROPOMI for both plumes were 0.5~1.5 km. Given the difference in definition for the aerosol height parameters between ALH and AEH, relatively high height values were retrieved from

GEMS compared to TROPOMI. In an ideal case under symmetric gaussian distribution with a width of 1 km, the AEH from GEMS was around 0.5 km higher than the peak height of aerosol layer. The ALH expresses the center (or peak) height, thus, the AEH from GEMS was overestimated by around 0.5 km relative to the ALH from TROPOMI. Although AEH had higher values than ALH from TROPOMI, the GEMS AEH retrievals for the dust transport case study were successfully retrieved.

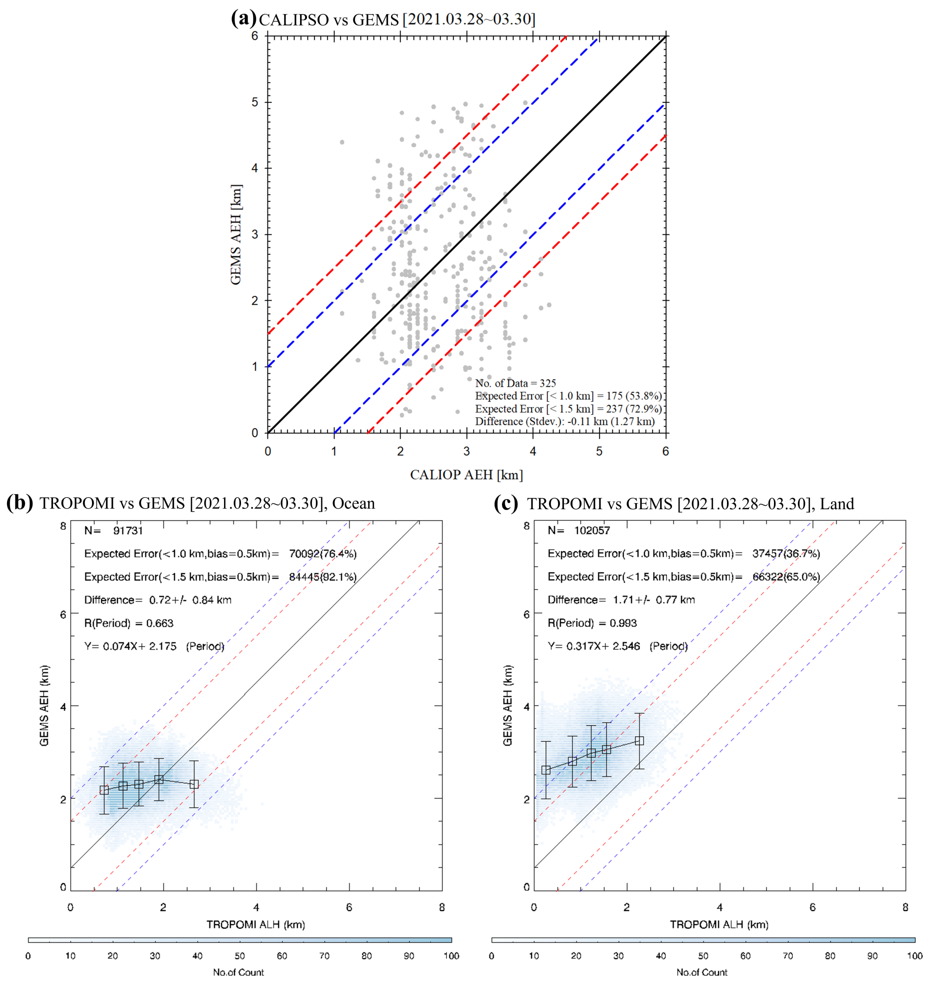

Figure 6. Intercomparison of (a) AEH between CALIOP and GEMS and (b) ALH from TROPOMI and AEH from GEMS over ocean and (c) over land (black dot and error bar is mean and standard deviation in 20% interval of each TROPOMI ALH) over the period from March 28 to 30, 2021.

Figure 6 shows intercomparison results for aerosol plume height among GEMS, CALIOP, and TROPOMI during the case study of yellow dust transport in East Asia from March 28 to 30, 2021. For the direct comparison shown in Figure 6a, the difference in AEH between GEMS and CALIOP was -0.11±1.27 km. Nanda *et al.* (2020) reported that the difference in ALH between TROPOMI and CALIOP was 0.53 km for 4 cases of thick Saharan dust plumes. In addition, 53.8% and 72.9% of the total pixels showed differences less than 1.0 and 1.5 km, respectively. Large AEH uncertainty occurred mostly over the inland area of China. Because AEH from GEMS uses only the O_2-O_2 absorption band, the accuracy of AEH is sensitive to uncertainty in surface reflectance and AOD. From Park et al. (2016), total error budget of AEH is 0.74~1.28 km, and the total error budget considered the uncertainty of AOD, SSA, aerosol particle size, and surface albedo in the aerosol retrieval process. The total error budget amount from the previous study is similar value of standard deviation of AEH difference between GEMS and CALIOP.

Figures 6b and 6c shows a comparison of GEMS and TROPOMI for the period of March 28 ~ 30, 2021 over land and ocean, respectively. The difference between GEMS AEH and TROPOMI ALH was 0.71 ± 0.84 km and 1.71 ± 0.77 km over ocean and land in this case, respectively. In addition, 82.4% and 37.3% of all pixels had differences less than 1.5 km over ocean and land, respectively. However, the ALH from TROPOMI is generally lower than the AEH from GEMS because of the discrepancy in definitions. Based on the assumption of aerosol vertical distribution for AEH retrieval, the difference between AEH and center height of aerosol extinction profile is around 0.5 km. To consider the inconsistency of definition between ALH and AEH, the difference between two retrieval results decreased to 0.5 km bias. After consideration of definition inconsistency, the proportion of pixels within the expected error ranges of 1.0 km are enhanced to 76.4% and 36.7% over ocean and land, respectively.

In addition, these proportion values have strong dependence of surface types. The proportion over land (over ocean) was lower (higher) than the corresponding result from the comparison of GEMS and CALIOP. The TROPOMI ALH from version 2 is strong surface type dependence as compared to the ground lidar data (Michailidis et al., 2023). However, the relationship between TROPOMI ALH and GEMS AEH in 20% interval of each TROPOMI ALH is 0.663 and 0.993 over ocean and land, respectively.

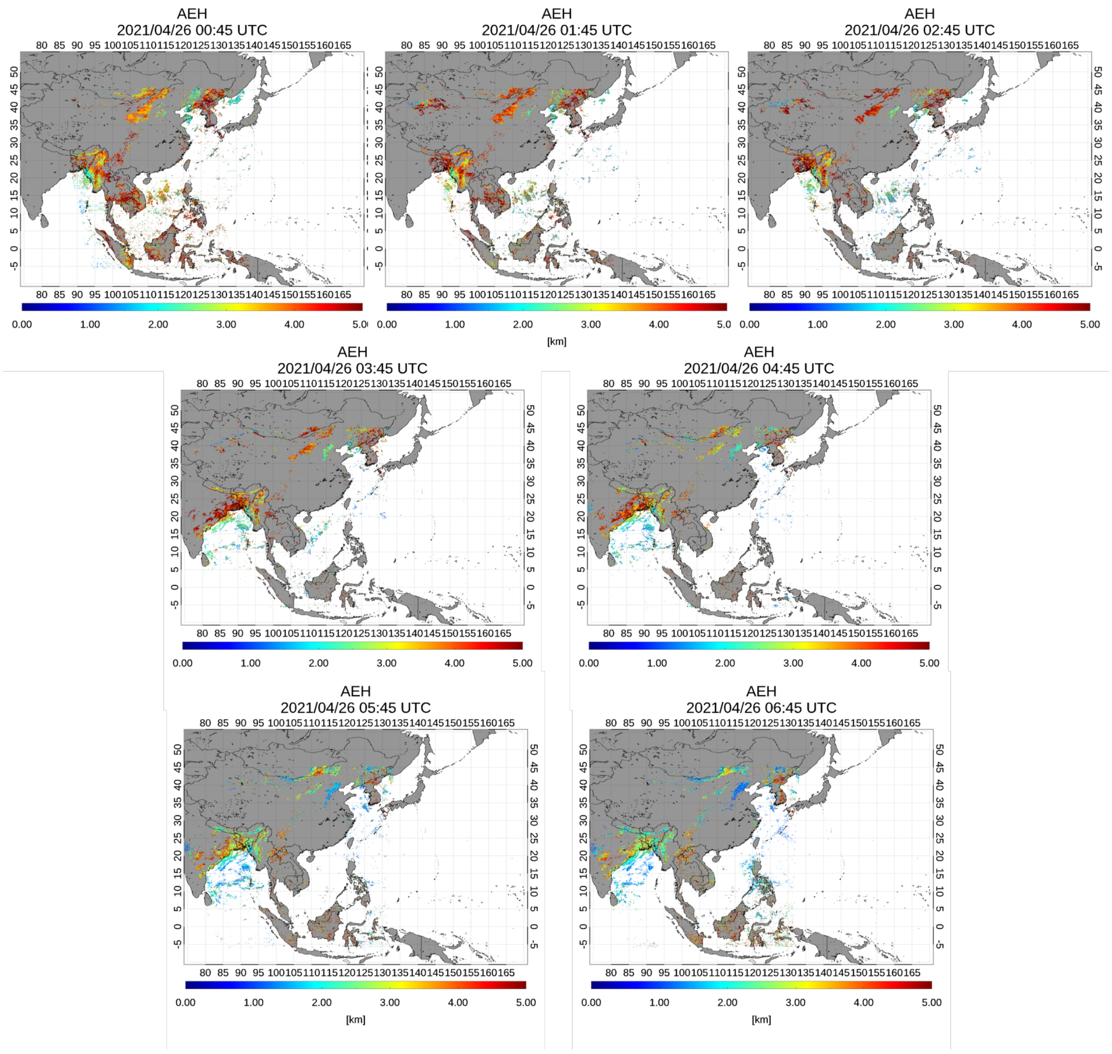

Figure 7. Case study results for AEH based on GEMS observations on April 26, 2021.

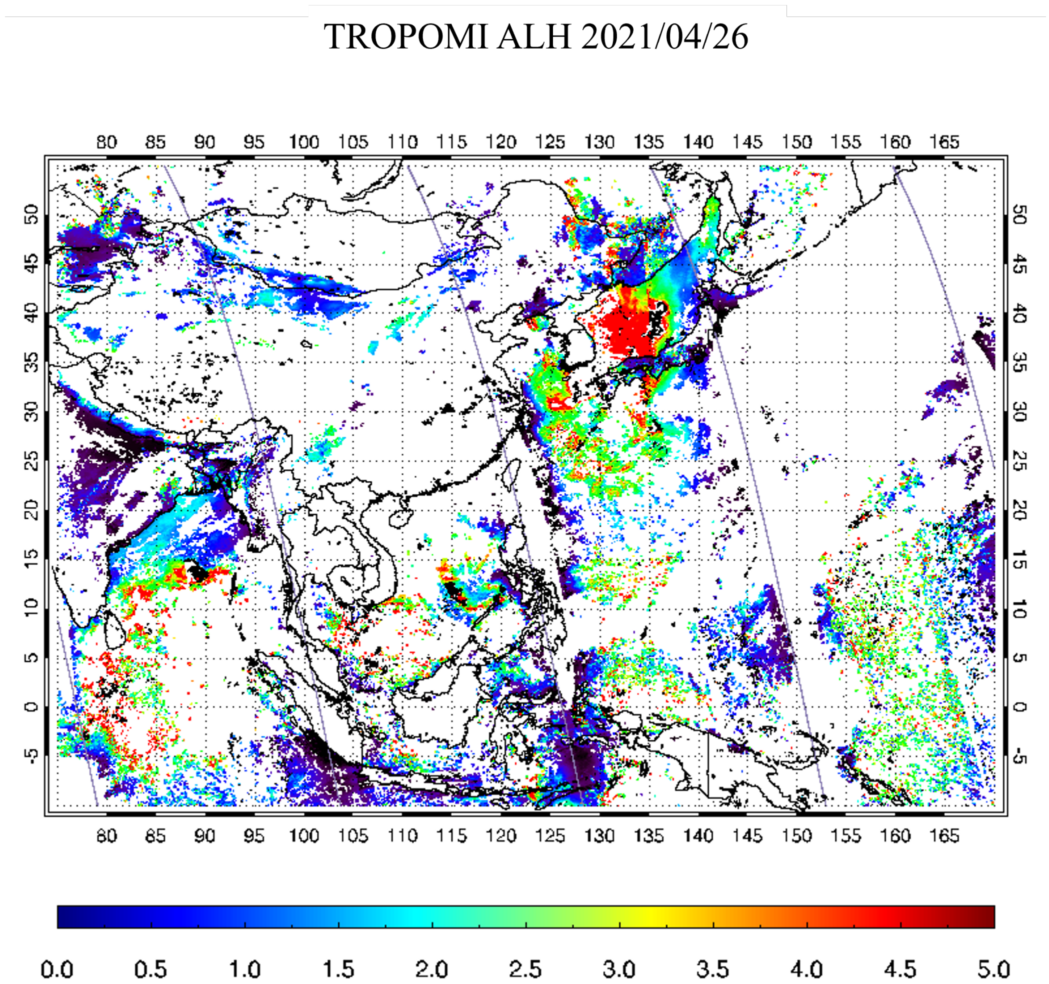

Figure 8. ALH retrieved from TROPOMI and orbit path of CALIOP on April 26, 2021 (Unit: km).

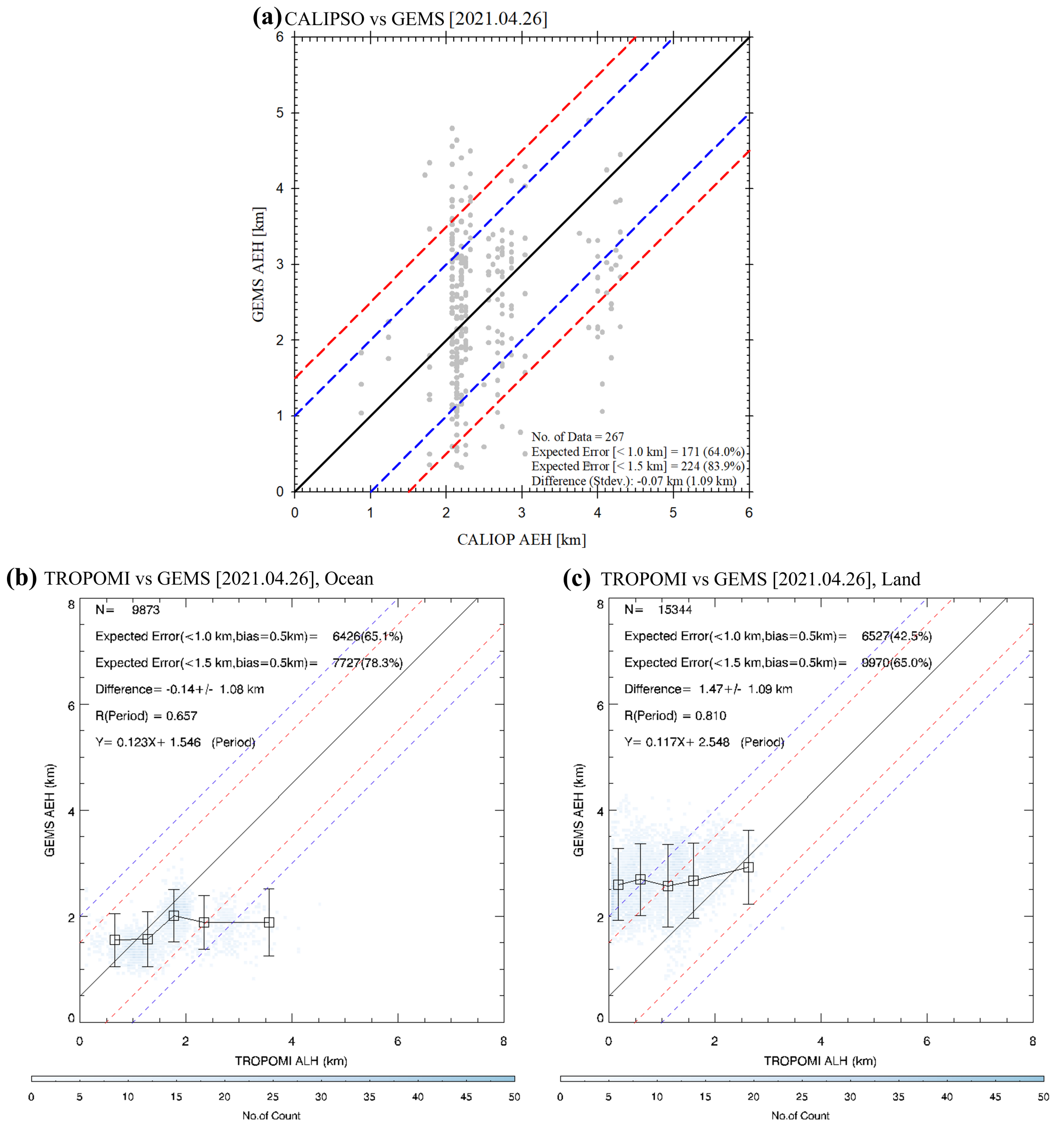

Figure 9. Intercomparison of (a) AEH between CALIOP and GEMS, and (b) ALH from TROPOMI and AEH from GEMS over ocean and (c) over land (black dot and error bar is mean and standard deviation in 20% interval of each TROPOMI ALH) on April 26, 2021.

An additional intercomparison case of April 26, 2021, is shown in Figures 7 (GEMS) and 8 (TROPOMI). During the transport of the yellow dust plume from inland China to the coastal area, AEH changed from 4.0 km at 02:00 UTC to 2.0 km at 06:00 UTC. By contrast, ALH from TROPOMI only observed the 1.5~2.5 km layer height over East Asia around 04:00 UTC. Although the AEH from GEMS had spatio-temporal uncertainty, this case demonstrates the advantage of AEH retrieval from GEMS for continuous monitoring of changes in plume height, in particular during dust transport. As shown in Figure 9, AEH from GEMS showed differences in height of -0.07 ± 1.09 km (compared to CALIOP). In addition, the differences in height of -0.14 ± 1.06 and 1.47 ± 1.09 km over ocean and land as compared to TROPOMI ALH.

From two different case results, proportion values within 1.0 km (or 1.5 km) height difference between TROPOMI and GEMS have strong dependence of surface types. The proportion over land (over ocean) was lower (higher) than the corresponding result from the comparison of GEMS and CALIOP. The TROPOMI ALH from version 2 is strong surface type dependence as compared to the ground lidar data (Michailidis et al., 2023). However, the relationship between TROPOMI ALH and GEMS AEH in 20% interval of each TROPOMI ALH have high correlation coefficients. In the case of March 28~30, the correlation coefficients between TROPOMI and GEMS are 0.663 and 0.993 over ocean and land, respectively. In the case of April 26, the correlation coefficients are 0.657 and 0.810 over ocean and land, respectively.

5. Long-term validation

For long-term validation, we used the AEH retrieval results from January to June, 2021. The CALIOP and TROPOMI satellites passed over the study area around 13:30 local time, which is around 04:30 UTC for East Asia and around 06:30 UTC for India. Most temporal colocation pixels aligned with observation times of 04:00~06:00 UTC, respectively. To check the dependence of several retrieval variables, the AI value for UV

(UVAI), AOD, SSA, and dominant aerosol type in each pixel (TYPE) were obtained from the L2AERAOD. Although the GEMS algorithm retrieved AEH in the range of 0~10 km, the sensitivity of O_2-O_2 SCD was weak in cases of high AEH because of the vertical distribution of air molecules. To ensure sufficient quality of retrieved data, therefore, the AEHs from GEMS and CALIOP, and the ALH from TROPOMI were used only in pixels where the AEH from GEMS were lower than 5 km.

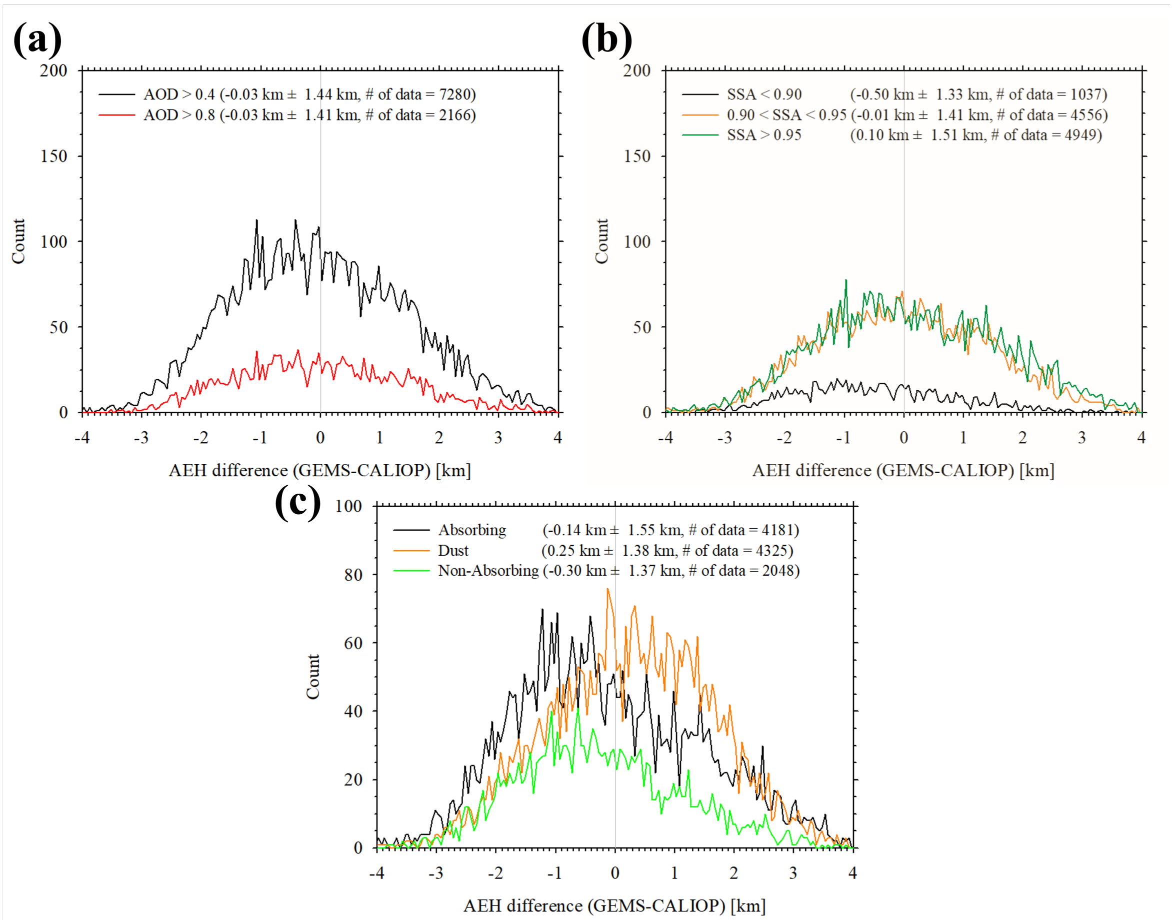

Figure 10. Histogram of AEH difference between CALIOP and GEMS with respect to (a) AOD, (b) SSA, and (c) TYPE from GEMS over the period from January 1 to June 30, 2021.

Figure 10 shows histograms of difference in AEH between GEMS and CALIOP according to AOD at 443 nm, SSA at 443 nm, and TYPE from GEMS. From Figure 10a, the dependence on AOD threshold was insignificant; the average estimated AEH difference was -0.03 km, but the variation in AEH difference was around 1.4 km based on the standard deviation for AOD > 0.4. Because of uncertainty in GEMS operational products, AEH from GEMS exhibits large variability. Although L2AERAOD from GEMS retrieved the AOD, SSA, and aerosol types, the retrieved results from L2AERAOD include significant uncertainty. Go et al. (2020) reported that the root-mean square error (RMSE) of AOD between MODIS and OMI UV aerosol algorithm is 0.276~0.341.

In addition, significant fitting error perturbs the fitting signals and tends to result in the underestimation of SCD. Although the fitting error of O_2-O_2 SCD from GEMS radiance was minimized, the fitting error is still remained around 6%, as indicated in Table 2. The discrepancy in fitting condition between the simulated and observed radiance biased the SCD estimation, which in turn led to bias and variation in the AEH retrieval. Combined with the high sensitivity of AEH errors to aerosol optical properties, uncertainty arising from L2AERAOD causes significant variability in AEH.

The variation in AEH difference between observation platforms is shown in Figure 10b as a histogram according to SSA threshold. Across the entire SSA threshold range, the standard deviation of the AEH difference was 1.33~1.51 km. In particular, this standard deviation decreased slightly with decreasing SSA. The aerosol height parameter is more sensitive to absorbing-dominant aerosols than scattering-dominant aerosols (e.g., Park *et al.*, 2016; Nanda *et al.*, 2020). For this reason, the variability of AEH is smaller in absorbing-dominant aerosols than scattering-dominant aerosols, if the uncertainty of other aerosol parameters (AOD, SSA, and TYPE) is the same conditions.

Figure 10c shows the dependence of AEH difference on TYPE. The TYPE product included dependence on the aerosol size and optical absorptivity. For this reason, the AEH difference graphs for the “Dust” and “Absorbing” types differ, despite both types being absorbing-dominant aerosols. The AEH difference for the “Absorbing” type showed a negative bias with a large standard deviation, whereas a positive bias with a small standard deviation was obtained for the “Dust” type. The AEH difference for the “Non-Absorbing” aerosol type showed the largest negative bias in this comparison. These results suggest that the aerosol size distribution of fine particles affects the negative bias of AEH. Combined with the AEH difference bias illustrated in Figure 8b, these findings indicate that the bias in AEH difference for “Absorbing” aerosols is weakened by their absorbing-dominant property.

Figure 11 shows means and standard deviations for AEH difference between CALIOP and GEMS according to AOD and AI values from GEMS. For AOD, the mean AEH difference ranged from -0.13 to 0.03 km with a standard deviation of approximately 1.45 km. Similar to Figure 11a, the variation in AEH difference with AOD change was insignificant. For AI, the smallest AEH difference was -0.19 km, obtained for the AI range of 1.5~2.0. The largest AEH difference was 0.24 km for the AI range of 4.0~4.5. Although the AEH difference varied slightly, no consistent tendency in AEH variation with AI was observed Overall, the standard deviation of AEH difference ranged from 1.49 km ($0.0 < AI < 0.5$) to 1.18 km ($4.5 < AI < 5.0$), and a consistent tendency of decreasing variance in AEH difference was found with increasing AI.

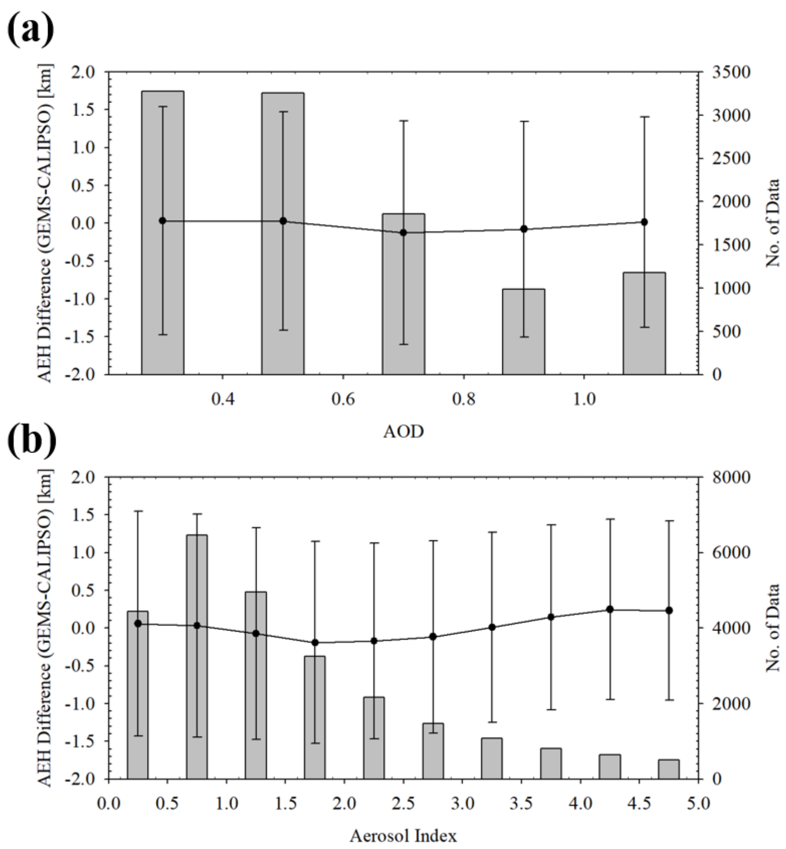

Figure 11. AEH difference between CALIOP and GEMS with respect to ranges of (a) AOD and (b) AI obtained from GEMS from January 1 to June 30, 2021 (line and error bar is the mean and standard deviation of AEH difference, and the box is number of data).

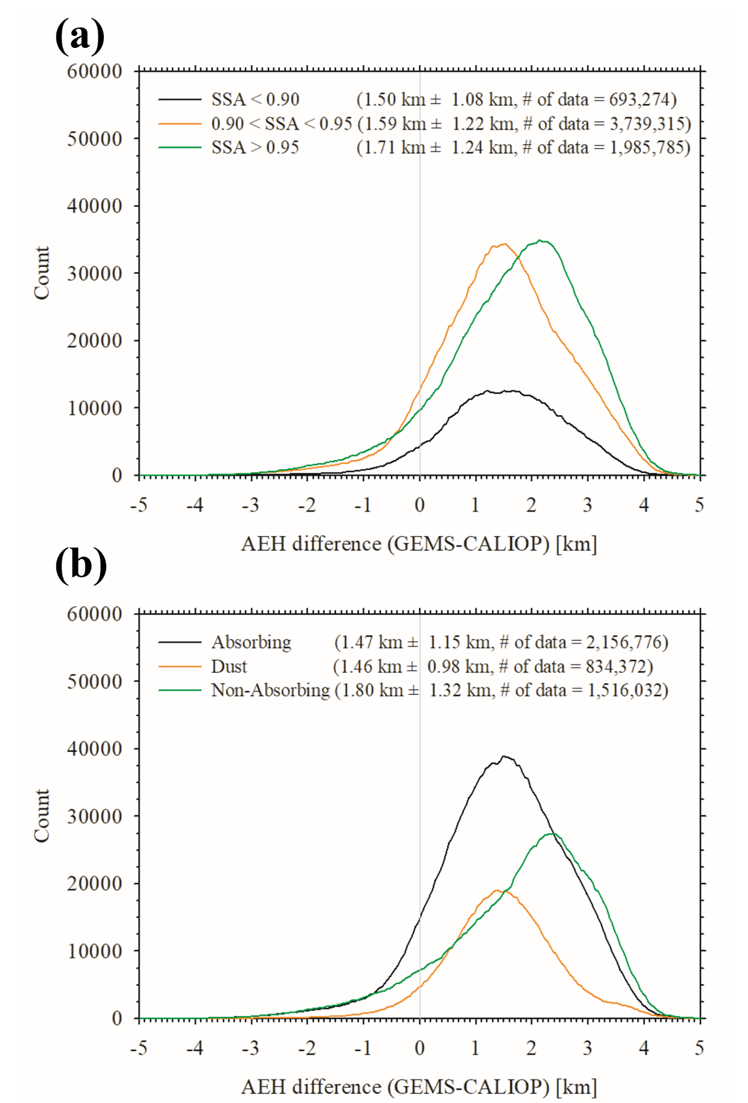

Figure 12. Histograms of differences between ALH from TROPOMI and AEH from GEMS [(AEH from GEMS) – (ALH from TROPOMI)] with respect to (a) SSA, and (b) TYPE from GEMS in the period from January 1 to June 30, 2021.

Figure 12 shows histograms of differences between ALH from TROPOMI and AEH from GEMS [(AEH from GEMS) – (ALH from TROPOMI)] according to the SSA and TYPE obtained from GEMS. The (AEH from GEMS) – (ALH from TROPOMI) depends on both SSA and TYPE. The mean value of (AEH from GEMS) – (ALH from

TROPOMI) decreased as the aerosol absorptivity increased. This difference was 1.50 ± 1.08, 1.59 ± 1.22, and 1.71 ± 1.24 km for pixels of SSA < 0.90, 0.90 < SSA < 0.95, and SSA > 0.95, respectively. Comparing these results to Figure 8b, we find that the standard deviation of the comparison with TROPOMI was approximately 75% of the corresponding value for CALIOP. It is because both TROPOMI and GEMS are passive sensors that use similar retrieval methods for oxygen absorption bands. Nanda *et al.* (2020) showed that the operational algorithm of TROPOMI operational algorithm can provide ALH pixel retrievals only for scenes dominated by absorbing aerosol particles. In addition, Griffin *et al.* (2020) reported that the pixels with small positive UVAI (weak absorbing cases) are identified with low QA values (QA ≤ 0.5) in the offline product of ALH. Although the TROPOMI ALH algorithm updates, the sensitivity of aerosol layer height information is fundamentally weak sensitivity in scattering dominant aerosols (e.g., Park et al., 2016). For this reason, the bias and standard deviation of height difference between GEMS and ALH is generally larger in high SSA.

In addition, (AEH from GEMS) – (ALH from TROPOMI) depends on TYPE, as shown in Figure 10b. The difference was 1.47 ± 1.15, 1.46 ± 0.98, and 1.80 ± 1.32 km for "Absorbing", "Dust", and "Non-Absorbing" type aerosols, respectively. Similar to Figure 8c, the TYPE dependence of aerosol height information was influenced by both absorptivity and size information. In addition, the difference in the definition of ALH from TROPOMI and AEH from GEMS impacted the comparison. "Dust" types of aerosol are mainly transported in the free troposphere with gaussian-like shapes, and the associated plume thickness is highly variable. However, "Absorbing" aerosols mainly originate from anthropogenic emissions in East Asia and mostly distributed near the surface with homogeneous concentration (e.g., Gao *et al.*, 2014; Wang *et al.*, 2012;

Peng *et al.*, 2016). Transport patterns and vertical distribution shape according to the aerosol types are affected to the accuracy of aerosol height retrieval results.

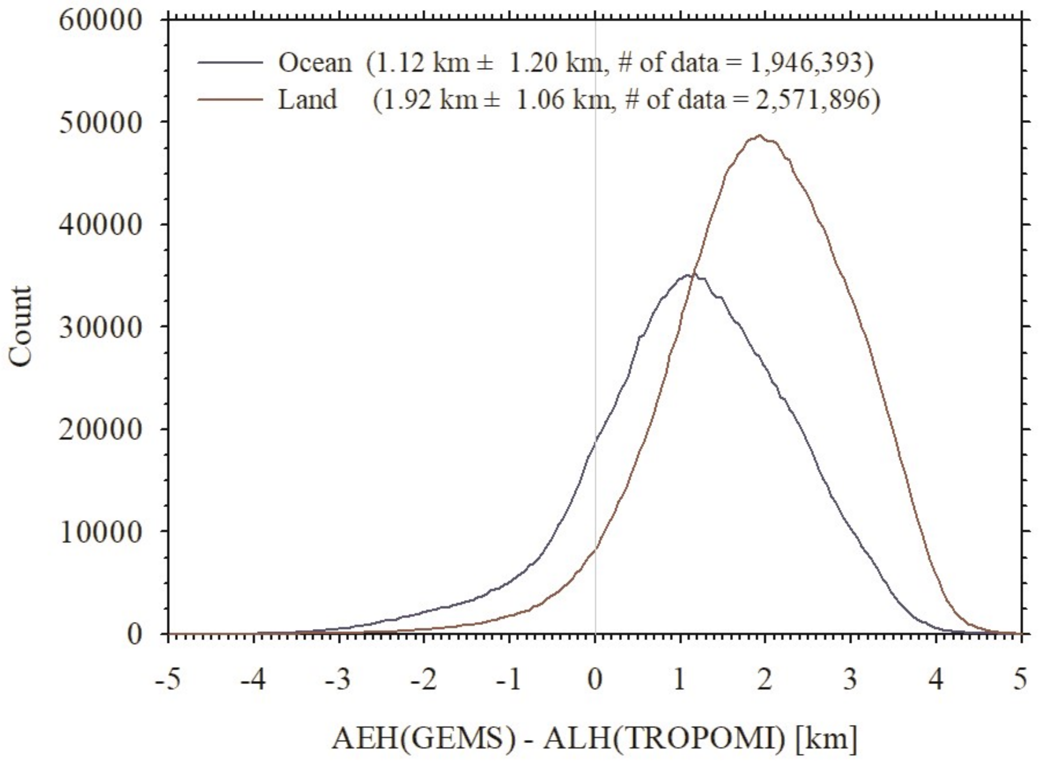

Figure 13. Histogram of the difference between ALH from TROPOMI and AEH from GEMS [(AEH from GEMS) – (ALH from TROPOMI)] over land and ocean pixels, respectively, from January 1 to June 30, 2021.

The non-Lambertian effect on the land surface impacted surface albedo uncertainty during AEH retrieval, and this effect led to bias and variance in AEH. In this study, the minimum Lambertian equivalent reflectance was used as the reference reflectance value. However, surface reflectivity has geometric dependence due to non-Lambertian effects, which leads to a bias of 0.01-0.02 for surface reflectance over the land surface (e.g., Qin *et al.*, 2019). To identify the sensitivity of surface property, a histogram was constructed of (AEH from GEMS) – (ALH from TROPOMI) after classification into land and ocean surface types, as shown in Figure 13. From the statistical results, the mean differences were estimated to be 1.09 ± 0.44 and 0.91 ± 0.93 km for ocean and land pixels, respectively, indicating insignificant difference in bias between these two surface covers. However, the standard deviation of the two surface types indicated a significant difference. Over the ocean surface, the histogram is very narrow. Although there are 6.5 times more data for land than those for the ocean surface, the land surface has a relatively wide histogram distribution. This discrepancy arises because the non-Lambertian effect causes bias in surface reflectance, while also influencing the variability in surface reflectance related to observation geometry. For this reason, land surface reflectance based on the non-Lambertian surface assumption is not fully representative of actual surface reflectance as a function of observation geometry. Therefore, the standard deviation of the layer height difference is larger over the land surface, and the significant difference between land and ocean pixels is mainly driven by the assumption of surface reflection properties.

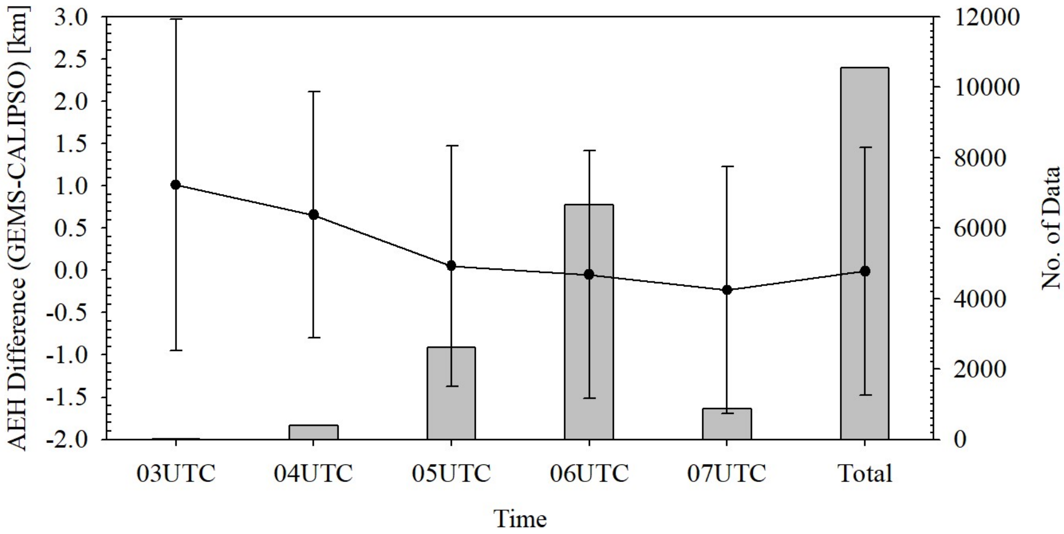

Figure 14. Diurnal dependence of AEH difference between CALIOP and GEMS from January 1 to June 30, 2021 (line and error bar is the mean and standard deviation of AEH difference, and the box is number of data).

The results of hourly statistical analyses are presented in Figure 14. Because they use a consistent definition of AEH, we show only a comparison of GEMS and CALIOP. The diurnal variation in AEH difference ranged from -0.23 ± 1.45 km (07:00 UTC, Number of Data = 867) to 1.01 ± 1.96 km (03:00 UTC, Number of Data = 23). However, the number of pixels observed at 03:00 UTC was insufficient for the identification of diurnal variation. The AEH difference of 0.66 ± 1.45 km was the next highest value obtained at 04:00 UTC (Number of Data = 395). The inhomogeneous number of data is mainly due to the lack of spatial homogeneity among retrieval pixels. Over India, very high AOD values were consistently observed during the comparison period. Otherwise, the AEH was only retrieved under conditions of severe anthropogenic emissions over East Asia. In addition, the diurnal variation in AEH difference was caused by spatial characteristics of AEH difference. From 03:00 to 05:00 UTC, CALIOP mainly passed over East Asia, which has numerous sources of aerosol emissions, including biomass burning, dust, and industrial activity. In addition, GEMS observed only the eastern part of India, which is dominated by anthropogenic aerosols. The spatial distribution of the dominant aerosol types may impact the diurnal variation in AEH difference.

6. Summary & Conclusions

Based on the possibility of retrieving AEH from environmental satellite sensors, an AEH retrieval algorithm for GEMS was developed that solely uses the O_2-O_2 absorption band with considering aerosol and surface properties. Because the sensitivity of AEH retrieval is strongly affected by optical amounts and properties of aerosols, as well as surface reflectivity, an AEH retrieval algorithm for GEMS was developed after retrieval of the GEMS operational algorithms, L2AERAOD and L2SFC. With the newly developed retrieval algorithm, GEMS can be used to monitor aerosol vertical information with high temporal and spatial resolution. To ensure significant sensitivity of AEH retrieval, only AEH retrieval results are with AOD larger than 0.3 were shown.

For dust plumes over East Asia, AEH retrieval results from GEMS indicated appropriated aerosol vertical information. After spatial and temporal colocation, the AEH from GEMS aligned well with the AEH information obtained from CALIOP. The differences in AEH between GEMS and CALIOP for dust plume cases were -0.07 ± 1.09 and -0.11 ± 1.27 km, with 53.8% and 72.9% of all pixels showing differences less than 1.0 and 1.5 km, respectively. Large AEH uncertainty was found mostly over inland China due to uncertainty in surface reflectance and AOD over the land surface. In addition, AEH from GEMS was overestimated compared to the TROPOMI ALH results.

The overestimation is partially caused by different definitions of ALH from TROPOMI and AEH from GEMS.

In long-term intercomparison with CALIOP, the average AEH difference was estimated to be -0.03 km, with variation of around 1.4 km based on the standard deviation for AOD > 0.4. In terms of sensitivity to surface albedo, the mean differences were estimated to be 1.09 and 0.91 km over the ocean and land, respectively, which is an insignificant difference of the biases between these two surface types. The large variation in AEH difference between GEMS and CALIOP was caused by uncertainty in the input parameters estimated from L2AERAOD and L2SFC. In the long-term intercomparison with TROPOMI, this difference was dependent on both SSA and TYPE. The difference was 1.50 ± 1.08 km, 1.59 ± 1.22 km, and 1.71 ± 1.24 km for pixels with SSA < 0.90, 0.90 < SSA < 0.95, and SSA > 0.95, respectively. In addition, differences of 1.47 ± 1.15 km, 1.46 ± 0.98 km, and 1.80 ± 1.32 km were obtained for the "Absorbing", "Dust", and the "Non-Absorbing" types of aerosols, respectively. The AEH difference ranged from -0.23 ± 1.45 km (07:00 UTC, Number of Data = 867) to 1.01 ± 1.96 km (03:00 UTC, Number of Data = 23), showing diurnal dependence. The spatial difference in dominant aerosol type may impact the diurnal variation in AEH difference.

The case studies and results of the long-term validation show that AEH retrieved from GEMS can provide information on aerosol vertical distribution, with applications in diverse research fields. The AEH results with the long-term statistical accuracy make possible to use the application study for AMF calculation of GEMS trace gas retrieval. In addition, AEH considerably affects the surface particulate matter (PM) concentration obtained from satellite-based AOD because PM estimation is significantly affected by the mixing layer height of aerosols. For this reason, the AEH can provide the effective mixing layer height of aerosols for anthropogenic aerosols, and also provide the vertical patterns for long-range transport of aerosols. By changing the transport patterns, the AEH can be identified the vertical distribution of aerosols by difference of AEH and ALH.

Although several fields of study may apply the AEH retrieval results, retrieval uncertainty in AEH remains due to the uncertainty of retrieved AOD and SSA. In addition, the uncertainty in surface reflectance and the discrepancy in O_2-O_2 SCD values between the simulation results and observations can be affected to the potential error sources of AEH from GEMS. To minimize the AEH retrieval uncertainty, further analysis related to the optimized input parameters of AOD, SSA, and aerosol type information is essential. Therefore, aerosol optical property retrieval by the visible channel will be needed for the further study. In addition, aerosol type is important input parameters to accurate estimation of AEH. Although the aerosol indices of UV and visible provide the aerosol type information, developing the aerosol type classification algorithm is necessary to make synergy with AEH retrieval. AEH provides representative layer height information as only one variable because of its sole reliance on O_2-O_2 SCD for direct estimation of aerosol height information. This method is limited to the consideration of aerosol vertical structures (i.e., Gaussian or exponential vertical distribution structures). Rather than using the GEMS sensor alone, using another absorption band for oxygen-based materials would provide additional scattering information about aerosols.

Data Availability

The TROPOMI ALH product is available from http://doi.org/10.5270/S5P-7g4iapn, and the CALIOP aerosol extinction profile product is available from https://doi.org/10.5067/CALIOP/CALIPSO/CAL_LID_L2_05kmAPro-Prov-V3-41. The GEMS AEH and AERAOD products are available from the Environmental Satellite Center in National Institute of Environmental Research (NIER) of the Republic of Korea.

Acknowledgements

This work was supported by the National Institute of Environment Research of the Republic of Korea under Grant NIER-2023-04-02-050.

References

Accarreta, J. R., de Haan, J. F., and Stammes, P.: Cloud pressure retrieval using the O2-O2 absorption band at 477 nm, J. Geophys. Res., 109, D05204, doi:10.1029/2003JD003915, 2004

Ahn, C., Torres, O., and Jethva, H.: Assessment of OMI near-UV aerosol optical depth over land, J. Geophys. Res., 119, 2457-2473, 2014.

Bogumil, K., Orphal, J., Burrows, J. P., and Flaud, J. M.: Vibrational progressions in the visible and near-ultraviolet absorption spectrum of ozone, Chem. Phys. Lett., 349, 241-248, 2001.

Buchard, V., de Silva, A. M., Colarco, P. R., Darmenov, A., Randles, C. A., Govindaraju, R., Torres, O., Campbell, J., and Spurr, R.: Using the OMI aerosol index and absorption aerosol optical depth to evaluate the NASA MERRA Aerosol reanalysis, Atmos. Chem. Phys., 15, 5743-5760, 2015.

Chen, X., Wang, J., Xu, X., Zhou, M., Zhang, H., Garcia, L. C., Colarco, P. R., Janz, S. J., Yorks, J., McGill, M., Reid, J. S., de Graaf, M., and Kondragunta, S.: First retrieval of absorbing aerosol height over dark target using TROPOMI oxygen B band: Algorithm development and application for surface particulate matter estimates, Remote Sens. Env., 265, 112674, 2021.

Chimot, J., Veefkind, J. P., Vlemmix, T., de Haan, J. F., Amiridis, V., Proestakis, E., Marinou, E., and Levelt, P. F.: An exploratory study on the aerosol height retrieval from OMI measurements of the 477 nm O2-O2 spectral band using a neural network approach, Atmos. Meas. Tech., 10, 783-809, 2017.

Choi, H., Liu, X., Abad, G. G., Seo, J., Lee, K. -M., and Kim, J.: A fast retrieval of cloud parameters using a Triplet of wavelengths of oxygen dimer band around 477 nm, Remote Sens., 13, 152, doi: 10.3390/rs13010152, 2021.

Choi, W., Lee, H., Kim, J., Ryu, J. -Y., Park, S. S., Park, J., and Kang, H.: Effects of spatiotemporal O4 column densities and temperature-dependent O4 absorption cross-section on an aerosol effective height retrieval algorithm using the O4 air mass factor from the ozone monitoring instrument, Remote Sens. Env., 229, 223-233, 2019.

Choi, W., Lee, H., and Kim, J.: First TROPOMI retrieval of aerosol effective height using O4 absorption band at 477 nm and aerosol classification, IEEE Trans. Geosci., Remote Sens., 59, 9873-9886, 2021.

de Graaf, M., Stammes, P., Torres, O., and Koelemeijer, R. B. A.: Absorbing aerosol index: Sensitivity analysis, application to GOME and comparison with TOMS, J. Geophys. Res., 110, D01201, doi:10.1029/2004JD005178, 2005.

de Graaf, M., de Haan, J. F., and Sanders, A. F. J.: TROPOMI ATBD of the Aerosol Layer Height, 75pp, Royal Netherlands Meteorological Institute, Netherland.

Ding, S., Wang, J., and Xu, X.: Polarimetric remote sensing in oxygen A and B bands: Sensitivity study and information content analysis for vertical profile of aerosols, Atmos. Meas. Tech, 9, 2077-2092, 2016.

Dubuisson, P., Frouin, R., Dessaily, D., Duforet, L., Leon, J. –F., Voss, K., and Antoine, D.: Estimating the altitude of aerosol plumes over the ocean from reflectance ratio measurements in the O2 A-band, Remote Sens. Environ., 113, 1899-1911, doi:10.1016/j.rse.2009.04.018, 2009.

European Space Agency*, TROPOMI Level 2 Aerosol Layer Height products. Version 02.* https://doi.org/10.5270/S5P-7g4iapn, 2021.

Gao, Y., Zhao, C., Liu, X., Zhang, M., and Leung, L. R.: WRF-Chem simulations of aerosols and anthropogenic aerosol radiative forcing in East Asia, Atmos. Environ., 92, 250-266, 2014.

Geddes, A., and Boesch, H.: Tropospheric aerosol profile information from high-resolution oxygen A-band measurements from space, Atmos. Meas. Tech., 8, 859-874, 2015.

Go, S., Kim, J., Park, S. S., Kim, M., Lim, H., Kim, J. -Y., Lee, D. -W., and Im, J.: Synergistic use of hyperspectral UV-visible OMI and broadband meteorological imager MODIS data for a merged aerosol product, Remote Sens., 12, 3987, doi:10.3390/rs12233987, 2020.

Griffin, D., Sioris, C., Chen, J., Dickson, N., Kovachik, A., de Graaf, M., Nanda, S., Veefkind, P., Dammers, E., McLinden, C. A., Makar, P., and Akingunola, A.: The 2018 fire season in North America as seen by TROPOMI: aerosol layer height intercomparisons and evaluation of model-derived plume heights, Atmos. Meas. Tech., 13, 1427-1445, 2020.

Herman, J. R., Bhartia, P. K., Torres, O., Hsu, C., Seftor, C., and Celarier, E.: Global distribution of UV-absorbing aerosols from Nimbus-7/TOMS data, J. Geophys. Res., 102(D14), 16911-16922, 1997.

Hong, H., Lee, H., Kim, J., Jeong, U., Ryu, J., and Lee, D. S.: Investigation of simultaneous effects of aerosol properties and aerosol peak height on the air mass factors for space-borne NO2 retrievals, Remote Sens., 9, 208, doi:10.3390/rs9030208, 2017.

Joiner, J., and Bhartia, P. K.: The determination of cloud pressures from rotational Raman scattering in satellite backscatter ultraviolet measurements, J. Geophys. Res., 100, 23019-23026, 1995.

Joiner, J., and Vasilkov, A. P.: First results from the OMI rotational Raman scattering cloud pressure algorithm, IEEE Trans. Geosci. Remote Sens., 44, 1272-1282, 2006.

Kim, M., Kim, J., Torres, O., Ahn, C., Kim, W., Jeong, U., Go, S., Liu, X., Moon, K. J., and Kim D. -R.: Optimal estimation-based algorithm to retrieve aerosol optical properties for GEMS measurements over Asia, 10, 162, doi:10.3390/rs10020162, 2018.

Kim, J., Jeong, U., Ahn, M. -H., Kim, J. H., Park, R. J., Lee, H., Song, C. H., Choi, Y. -S., Lee, K. -H., Yoo, J. -M., Jeong, M. -J., Park, S. K., Lee, K. -M., Song, C. -K., Kim, S. -W., Kim, Y. J., Kim, S. -W., Kim, M., Go, S., Liu, X., Chance, K., Chan Miller, C., Al-Saadi, J., Veihelmann, B., Bhartia, P. K., Torres, O., González Abad, G., Haffner, D. P., Ko, D. H., Lee, S. H., Woo, J. -H., Chong, H., Park, S. S., Nicks, D., Choi, W. J., Moon, K. -J., Cho, A., Yoon, J., Kim, S. -K., Hong, H., Lee, K., Lee, H., Lee, S., Choi, M., Veefkind, P., Levelt, P. F., Edwards, D. P., Kang, M., Eo, M., Bak, J., Baek, K., Kwon, H. -A., Yang, J., Park, J., Han, K. M., Kim, B. -R., Shin, H. -W., Choi, H., Lee, E., Chong, J., Cha, Y., Koo, J. -H., Irie, H., Hayashida, S., Kasai, Y., Kanaya, Y., Liu, C., Lin, J., Crawford, J. H., Carmichael, G. R., Newchurch, M. J., Lefer, B. L., Herman, J. R., Swap, R. J., Lau, A. K. H., Kurosu, T. P., Jaross, G., Ahlers, B., Dobber, M., McElroy, C. T., and Choi, Y.: New era of air quality from Space: Geostationary Environment Monitoring Spectrometer (GEMS), Bul. Ame. Meteorol. Soc., 101(1), E1–E22, 2020.

Kokhanovsky, A. A., and Rozanov, V. V.: The determination of dust cloud altitudes from a satellite using hyperspectral measurements in the gaseous absorption band, Int. J. Rem. Sens., 31, Nos. 9-10, 2729-2744, 2010.

Kooreman, M. L., Stammes, P., Trees, V., Sneep, M., Tilstra, L. G., de Graaf, M., Zweers, D. C. S., Wang, P., Tuinder, O. N. E., and Veefkind, J. P.: Effects of cloud on the UV absorbing aerosol index from TROPOMI, Atmos. Meas. Tech., 13, 6407-6426, 2020.

Lee, J., Kim, J., Song, C. H., Kim, S. B., Chun, Y., Sohn, B. J., and Holben, B. N.: Characteristics of aerosol types from AERONET sunphotometer measurements. Atmos. Env., 44, 3110-3117, 2010.

Lorente, A., Boersma, K. F., Yu, H., Doerner, S., Hilboll, A., Richter, A., Liu, M., Lamsal, L. N., Barkley, M., De Smedt, I., Van Roozendael, M., Wang, Y., Wagner, T., Beirle, S., Liu, J. -T., Krotkov, N., Stammes, P., Wang, P., Eskes, H. J., and Krol, M.: Structural uncertainty in air mass factor calculation for NO2 and HCHO satellite retrieval, Atmos. Meas. Tech., 10, 759-782, 2017.

Michailidis, K., Koukouli, M. -E., Balis, D., Veefkind, J. P., de Graaf, M., Mona, L., Papagianopoulos, N., Pappalardo, G., Tsikoudi, I., Amiridis, V., Marinou, E., Gialitaki, A., Mamouri, R. -E., Nisantzi, A., Bortoli, D., Joao Costa, M., Salgueiro, V., Papayannis, A., Mylonaki, M., Alados-Arboledas, L., Romano, S., Perrone, M. R., and Baars, H.: Validation of the TROPOMI/S5P aerosol layer height using EARLINET lidars, Atmos. Chem. Phys., 23, 1919-1940, 2023.

Nanda, S., de Graaf, M., Sneep, M., de Haan, J. F., Stammes, P., Sanders, A. F. J., Tuinder, O., Veefkind, J. P., and Levelt, P. F.: Error sources in the retrieval of aerosol information over bright surfaces from satellite measurements in the oxygen A band, Atmos. Meas. Tech., 11, 161–175, https://doi.org/10.5194/amt-11-161-2018, 2018.

Nanda, S., de Graaf, M., Veefkind, J. P., Sneep, M., ter Linden, M., Sun, J., and Level, P. F.: A first comparison of TROPOMI aerosol layer height (ALH) to CALIOP data, Atmos. Meas. Tech., 13, 3043-3059, 2020.

National Institute of Environmental Research, Geostationary Environment Monitoring Spectrometer (GEMS) Algorithm Theoretical Basis Document: Aerosol Retrieval Algorithm, 42pp, Ministry of Environment, Korea, 2020a.

National Institute of Environmental Research, Geostationary Environment Monitoring Spectrometer (GEMS) Algorithm Theoretical Basis Document: Surface Reflectance Algorithm, 35pp, Ministry of Environment, Korea, 2020b.

Omar, A., Winker, D. M., Vaughan, M. A., Ju, Y., Trepte, C. R., Ferrare, R. A., Lee, K.-P., Hostetler, C. A., Kittaka, C., Rogers, R. R., Kuehn, R. E., and Liu, Z.: The CALIPSO automated aerosol classification and Lidar ratio selection algorithm, J. Atmos. Ocean. Tech., 26, 10, 1994-2014, 2009.

Park, S. S., Kim, J., Lee, H., Torres, O., Lee, K. –M., and Lee, S. D.: Utilization of O4 slant column density to derive aerosol layer height from a space-borne UV-visible hyperspectral sensor: Sensitivity and case study, Atmos. Chem. Phys., 16, 1987-2006, doi:10.5194/acp-16-1987-2016, 2016.

Park, S. S., Takemura, T., and Kim, J.: Effect of temperature-dependent cross sections on O4 slant column density estimation by a space-borne UV-visible hyperspectral sensor, Atmos. Environ., 152, 98-110, 2017.

Park, S. S., Kim, S. -W., Song, C. -K., Park, J. -U., and Bae, K. -H.: Spatio-temporal variability of aerosol optical depth, total ozone, and NO2 over East Asia: Strategy for the validation to the GEMS Scientific Products, Remote Sens., 12, 2256, 2020.

Peng, J., Hu, M., Guo, S., Du, Z., Zheng, J., Shang, D., Zamora, M. L., Zeng, L., Shao, M., Wu, Y. -S., Zheng, J., Wang, Y., Glen, C. R., Collins, D. R., Molina, M. J., and Zhang R.: Markedly enhanced absorption and direct radiative forcing of black carbon under polluted urban environments, Proc. Natl. Acad. Sci., 113, 4266-4271, 2016.

Penning de Vries, M. J. M., Beirle, S., and Wagner, T.: UV aerosol indices from SCIAMACHY: Introducing the Scattering Index (SCI), Atmos. Chem. Phys., 9, 9555-9567, 2009.

Penning de Vries, M. J. M., Beirle, S., Hoermann, C., Kaiser, J. W., Stammes, P., Tilstra, L. G., Tuinder, O. N. E., and Wagner, T.: A global aerosol classification algorithm incorporating multiple satellite data sets of aerosol and trace gas abundances, Atmos. Chem. Phys., 15, 10597-10618, 2015.

Prospero, J. M., Ginoux, P., Torres, O., Nicholson, S. E., and Gill T. E.: Environmental characterization of global sources of atmospheric soil dust identified with the

Nimbus 7 total ozone mapping spectrometer (TOMS) absorbing aerosol product, Rev. Geophys., 40, 1002, doi:10.1029/2000RG000095, 2002.

Qin, W., Fasnacht, Z., Haffner, D., Vasilkov, A., Joiner, J., Krotkov, N., Fisher, B., and Spurr, R.: A geometry-dependent surface Lambertian-equivalent reflectivity product for UV-vis retrievals – Part 1: Evaluation over land surfaces using measurements from OMI at 466 nm, Atmos. Meas. Tech., 12, 3997-4017, 2019.

Rana, A., Jia, S., and Sarkar, S.: Black carbon aerosol in India: A comprehensive review of current status and future prospects, Atmos. Res., 218, 207-230, 2019.

Sanders, A. F. J., de Haan, J. F., Sneep, M., Apituley, A., Stammes, P., Vieitez, M. O., Tilstra, L. G., Tuinder, O. N. E., Koning, C. E., and Veefkind, J. P.: Evaluation of the operational Aerosol Layer Height retrieval algorithm for Sentinel-5 Precursor: application to O2 A band observations from GOME-2A, Atmos. Meas. Tech., 8, 4947-4977, 2015.

Sanders, A. F. J. and de Haan, J. F.: TROPOMI ATBD of the Aerosol Layer Height product, available at: http://www.tropomi.eu/sites/default/files/files/S5P-KNMI-L2-0006-RP-TROPOMI_ATBD_Aerosol_Height-v1p0p0-20160129.pdf (last access: 8 June 2020), 2016.

Sanghavi, S., Martonchik, J. V., Landgraf, J., and Platt, U.: Retrieval of optical depth and vertical distribution of particulate scatterers in the atmosphere using O2 A- and B-band SCIAMACHY observations over Kanpur: A case study, Atmos. Meas. Tech., 5, 1099-1119, 2012.

Spurr, R. "User's Guide VLIDORT Version 2.6, RT Solutions.", Cambridge, MA, USA, 2013.

Thalman, R., and Volkamer, R.: Temperature dependent absorption cross-sections of O2-O2 collision pairs between 340 and 630 nm and at atmospherically relevant pressure. Phys. Chem. Chem. Phys. 15, 15371e15381, 2013.

Torres, O., Bhartia, P. K., Herman, J. R., Ahmad, Z., and Gleason, J.: Derivation of aerosol properties from satellite measurements of backscattered ultraviolet radiation: Theoretical basis, J. Geophys. Res., 103(14), 17099-17110, 1998.

Torres, O., Decae, R., Veefkind, P., and de Leeuw, G.: OMI Aerosol Retrieval Algorithm, OMI Algorithm Theoretical Basis Document, Vol. III, Clouds, Aerosols and Surface UV Irradiance, NASA-KNMI ATBD-OMI-03, pp. 47-71, 2002.

Torres, O., Jethva, H., Ahn, C., Jaross, G., and Loyola, D. G.: TROPOMI aerosol products: evaluation and observations of synoptic-scale carbonaceous aerosol plumes during 2018-2020, Atmos. Meas. Tech., 13, 6789-6806, 2020.

Vandaele, A. C., Hermans, C., Simon, P. C., Carleer, M., Colin, R., Fally, S., Merienne, M. F., Jenouvrier, A., and Coquart, B.: Measurements of the NO2 absorption cross-section from 42000 cm-1 to 10000 cm-1 (238-1000 nm) at 220 K and 294 K, J. Quant. Spectrosc. Radiat. Transfer, 59, 3-5, 171-184, 1998.

Vasilkov, A., Joiner, J., Spurr, R., Bhartia, P. K., Levelt, P., and Stephens, G.: Evaluation of the OMI cloud pressures derived from rotational Raman scattering by comparisons with other satellite data and radiative transfer simulations, J. Geophys. Res., 113, D15S19, doi:10.1029/2007JD008689, 2008.

Vasilkov, A., Yang, E. -S., Marchenko, S., Qin, W., Lamsal, L., Joiner, J., Krotkov, N., Haffner, D., Bhartia, P. K., and Spurr, R.: A cloud algorithm based on the O2-O2 477 nm absorption band featuring an advanced spectral fitting method and the use of surface geometry-dependent Lambertian-equivalent reflectivity, Atmos. Meas. Tech., 11, 4093-4107, 2018.

Veefkind, J. P., Aben, I., McMullan, K., Foerster, H., de Vries, J., Otter, G., Claas, J., Eskes, H. J., de Haan, J. F., Kleipool, Q., van Weele, M., Hasekamp, O., Hoogeveen, R., Landgraf, J., Snel, R., Tol, P., Ingmann, P., Voors, R., Kruizinga, B., Vink, R., Visser, H., and Levelt, P. F.: TROPOMI on the ESA Sentinel-5 Precursor: A GMES mission for global observations of the atmospheric composition for climate, air quality and ozone layer applications, Remote Sens. Env., 120, 70-83, 2012.

Veihelmann, B., Levelt, P. F., Stammes, P., and Veefkind, J. P.: Simulation study of the aerosol information content in OMI spectral reflectance measurements, Atmos. Chem. Phys., 7, 3115-3127, 2007.

Wang, R., Tao, S., Wang, W., Liu, J., Shen, H., Shen, G., Wang, B., Liu, X., Li, W., Huang, Y., Zhang, Y., Lu, Y., Chen, H., Chen, Y., Wang, C., Zhu, D., Wang, X., Li, B., Liu, W., and M, J.: Black carbon emissions in China from 1949 to 2050, Environ., Sci. Technol., 46, 7595-7603, 2012.

Winker, D. M., Vaughan, M. A., Omar, A. H., Hu, Y., Powell, K. A., Liu, Z., Hunt, W. H., and Young, S. A.: Overview of the CALIPSO mission and CALIOP data processing algorithms, J. Atmos. Oceanic Technol., 26, 2310-2323, 2009.

Zeng, Z. -C., Chen, S., Natraj, V., Le, T., Xu, F., Merrelli, A., Crisp, D., Sander, S. P., and Yung, Y. L.: Constraining the vertical distribution of coastal dust aerosol using OCO-2 O2 A-band measurements, Remote Sens. Env., 236, 111494, 2020.